




TECH BRIEFS

NATIONAL AERONAUTICS AND SPACE ADMINISTRATION

-  **Technology Focus**
-  **Electronics/Computers**
-  **Software**
-  **Materials**
-  **Mechanics/Machinery**
-  **Manufacturing**
-  **Bio-Medical**
-  **Physical Sciences**
-  **Information Sciences**
-  **Books and Reports**

INTRODUCTION

Tech Briefs are short announcements of innovations originating from research and development activities of the National Aeronautics and Space Administration. They emphasize information considered likely to be transferable across industrial, regional, or disciplinary lines and are issued to encourage commercial application.

Availability of NASA Tech Briefs and TSPs

Requests for individual Tech Briefs or for Technical Support Packages (TSPs) announced herein should be addressed to

National Technology Transfer Center

Telephone No. (800) 678-6882 or via World Wide Web at www2.nttc.edu/leads/

Please reference the control numbers appearing at the end of each Tech Brief. Information on NASA's Innovative Partnerships Program (IPP), its documents, and services is also available at the same facility or on the World Wide Web at <http://ipp.nasa.gov>.

Innovative Partnerships Offices are located at NASA field centers to provide technology-transfer access to industrial users. Inquiries can be made by contacting NASA field centers listed below.

NASA Field Centers and Program Offices

Ames Research Center

Lisa L. Lockyer
(650) 604-1754
lisa.l.lockyer@nasa.gov

Dryden Flight Research Center

Gregory Poteat
(661) 276-3872
greg.poteat@dfrc.nasa.gov

Glenn Research Center

Kathy Needham
(216) 433-2802
kathleen.k.needham@nasa.gov

Goddard Space Flight Center

Nona Cheeks
(301) 286-5810
nona.k.cheeks@nasa.gov

Jet Propulsion Laboratory

Ken Wolfenbarger
(818) 354-3821
james.k.wolfenbarger@jpl.nasa.gov

Johnson Space Center

Michele Brekke
(281) 483-4614
michele.a.brekke@nasa.gov

Kennedy Space Center

David R. Makufka
(321) 867-6227
david.r.makufka@nasa.gov

Langley Research Center

Martin Waszak
(757) 864-4015
martin.r.waszak@nasa.gov

Marshall Space Flight Center

Jim Dowdy
(256) 544-7604
jim.dowdy@msfc.nasa.gov

Stennis Space Center

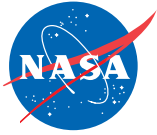
John Bailey
(228) 688-1660
john.w.bailey@nasa.gov

Carl Ray, Program Executive

Small Business Innovation
Research (SBIR) & Small
Business Technology
Transfer (STTR) Programs
(202) 358-4652
carl.g.ray@nasa.gov

Doug Comstock, Director

Innovative Partnerships
Program Office
(202) 358-2560
doug.comstock@nasa.gov



TECH BRIEFS

NATIONAL AERONAUTICS AND SPACE ADMINISTRATION



5 Technology Focus: Test & Measurement

- 5 Torque Sensor Based on Tunnel-Diode Oscillator
- 5 Shaft-Angle Sensor Based on Tunnel-Diode Oscillator
- 6 Ground Facility for Vicarious Calibration of Skyborne Sensors
- 7 Optical Pressure-Temperature Sensor for a Combustion Chamber
- 7 Impact-Locator Sensor Panels



9 Electronics/Computers

- 9 Low-Loss Waveguides for Terahertz Frequencies
- 10 MEMS/ECD Method for Making $\text{Bi}_{2-x}\text{Sb}_x\text{Te}_3$ Thermoelectric Devices
- 11 Low-Temperature Supercapacitors
- 12 Making a Back-Illuminated Imager With Back-Side Contact and Alignment Markers
- 13 Compact, Single-Stage MMIC InP HEMT Amplifier
- 14 $\text{Nb}_x\text{Ti}_{1-x}\text{N}$ Superconducting-Nanowire Single-Photon Detectors



15 Manufacturing & Prototyping

- 15 Improved Sand-Compaction Method for Lost-Foam Metal Casting
- 16 Improved Probe for Evaluating Compaction of Mold Sand



17 Materials

- 17 Polymer-Based Composite Catholytes for Li Thin-Film Cells
- 17 Using ALD To Bond CNTs to Substrates and Matrices
- 18 Alternating-Composition Layered Ceramic Barrier Coatings



21 Mechanics/Machinery

- 21 Variable-Structure Control of a Model Glider Airplane
- 21 Axial Halbach Magnetic Bearings
- 22 Compact, Non-Pneumatic Rock-Powder Samplers



25 Bio-Medical

- 25 Biochips Containing Arrays of Carbon-Nanotube Electrodes



27 Physical Sciences

- 27 $\text{Nb}_x\text{Ti}_{1-x}\text{N}$ Superconducting-Nanowire Single-Photon Detectors
- 27 Neon as a Buffer Gas for a Mercury-Ion Clock
- 27 Miniature Incandescent Lamps as Fiber-Optic Light Sources
- 28 Bidirectional Pressure-Regulator System
- 29 Prism Window for Optical Alignment
- 30 Single-Grid-Pair Fourier Telescope for Imaging in Hard-X Rays and γ Rays
- 31 Range-Gated Metrology With Compact Optical Head



33 Information Sciences

- 33 Lossless, Multi-Spectral Data Compressor for Improved Compression for Pushbroom-Type Instruments

This document was prepared under the sponsorship of the National Aeronautics and Space Administration. Neither the United States Government nor any person acting on behalf of the United States Government assumes any liability resulting from the use of the information contained in this document, or warrants that such use will be free from privately owned rights.



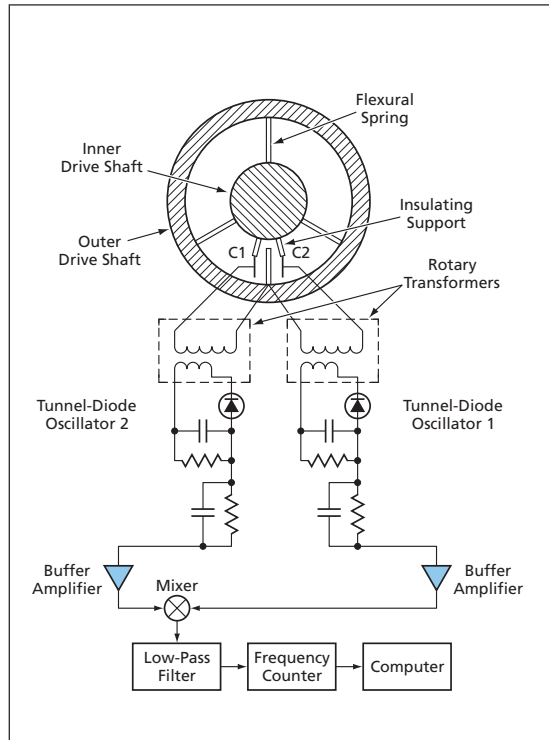
Torque Sensor Based on Tunnel-Diode Oscillator

This sensor would function over a wide temperature range.

NASA's Jet Propulsion Laboratory, Pasadena, California

A proposed torque sensor would be capable of operating over the temperature range from 1 to 400 K, whereas a typical commercially available torque sensor is limited to the narrower temperature range of 244 to 338 K. The design of this sensor would exploit the wide temperature range and other desirable attributes of differential transducers based on tunnel-diode oscillators as described in "Multiplexing Transducers Based on Tunnel-Diode Oscillators" (NPO-43079), *NASA Tech Briefs*, Vol. 30, No. 9 (September 2006), page 42.

The proposed torque sensor (see figure) would include three flexural springs that would couple torque between a hollow outer drive shaft and a solid inner drive shaft. The torque would be deduced from the torsional relative deflection of the two shafts, which would be sensed via changes in capacitances of two capacitors (C1 and C2) defined by two electrodes attached to the inner shaft and a common middle electrode attached to the outer shaft. Each capacitor would be part of a tunnel-diode oscillator circuit. Each



Torque Would Bend the Flexural Springs, causing a slight relative rotation of the inner and outer shafts, thereby increasing one of the capacitances and decreasing the other one, thereby further causing a decrease in the frequency of one tunnel-diode oscillator and an increase in the frequency of the other one.

capacitor would be coupled to the rest of its oscillator circuit via a rotary transformer, so that there would be no need for wire connections between the shaft and the stationary part of the affected machine.

The sensory principle would be mostly the same as that described in the cited prior article. At zero torque, the flexural springs would cause the common middle electrode to lie midway between the C1 and C2 electrodes. The two capacitances, and thus the frequencies of the two oscillators, would vary in opposite directions as torque caused the middle electrode to move away from the midpoint. The outputs of the tunnel-diode oscillators would be mixed and low-pass filtered to obtain a signal at the difference between the frequencies of the two oscillators. The difference frequency would be measured by a frequency counter and converted to torque by a computer.

This work was done by Talso Chui and Joseph Young of Caltech for NASA's Jet Propulsion Laboratory. Further information is contained in a TSP (see page 1). NPO-43325

Shaft-Angle Sensor Based on Tunnel-Diode Oscillator

Advantages would include relative simplicity and low-temperature capability.

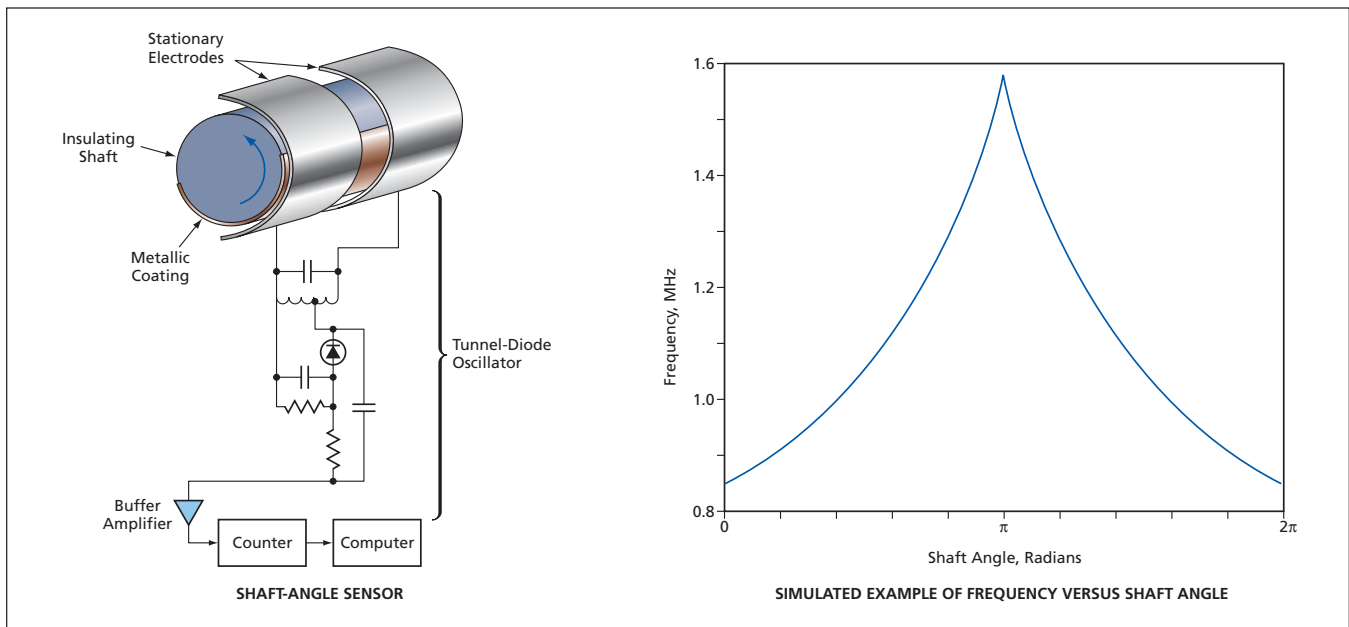
NASA's Jet Propulsion Laboratory, Pasadena, California

A proposed brushless shaft-angle sensor for use in extreme cold would offer significant advantages over prior such sensors:

- It would be capable of operating in extreme cold; and
- Its electronic circuitry would be simpler than that of a permanent-magnet/multiple-Hall-probe shaft-angle sensor that would otherwise ordinarily be used to obtain comparable angular resolution.

As in the case described in the immediately preceding article, the design of this sensor would exploit the wide temperature range and other desirable attributes of differential transducers based on tunnel-diode oscillators as described in "Multiplexing Transducers Based on Tunnel-Diode Oscillators" (NPO-43079), *NASA Tech Briefs*, Vol. 30, No. 9 (September 2006), page 42.

The principle of operation of the proposed shaft-angle sensor requires that the shaft (or at least the portion of the shaft at the sensor location) be electrically insulating. The affected portion of the shaft would be coated with metal around half of its circumference. Two half-circular-cylinder electrodes having a radius slightly larger than that of the shaft would be mounted on the stator, concentric with



The **Series Capacitance** between the stationary electrodes would vary as the shaft turned, causing the frequency of the tunnel-diode oscillator to vary.

the shaft, so that there would be a small radial gap between them and the outer surface of the shaft. Hence, there would be a capacitance between each stationary electrode and the metal coat on the shaft.

The stationary electrodes would be connected into a tunnel-diode oscillator circuit, so that the series combination of the two capacitances would be part of

the capacitance that determines the oscillation frequency. As the shaft is rotated, the stationary-electrode/metal-coat overlap area would change, causing the series capacitance and the oscillation frequency to change. The frequency would be measured and used to infer the shaft angle from the known relationships among shaft angle, capacitance, and frequency.

It should be noted that a given frequency could signify either of two distinct shaft angles. If necessary, one could resolve the shaft-angle ambiguity by use of two sensors at different angular positions.

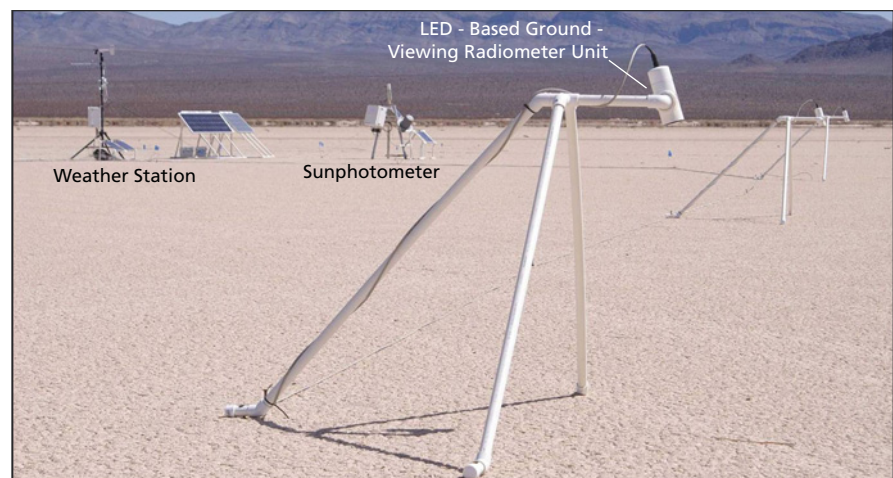
This work was done by Talso Chui of Caltech for NASA's Jet Propulsion Laboratory. Further information is contained in a TSP (see page 1). NPO-43328.

Ground Facility for Vicarious Calibration of Skyborne Sensors

This is an automated facility that generates Web-accessible data.

NASA's Jet Propulsion Laboratory, Pasadena, California

An automated ground facility, for vicarious radiometric calibration of airborne and spaceborne sensors of visible and infrared light has been established. In the term "vicarious calibration," "vicarious" is used in the sense of "in place of another," signifying "in place of laboratory calibration." Vicarious calibration involves the use of ground truth in the form of measurements by ground-viewing radiometers, a Sun-viewing photometer, and meteorological instruments positioned in a ground target area. Typically, the target is a dry lakebed or other relatively homogeneous area. (The value of a relatively homogeneous target is that it minimizes effects of errors of registration between the target and the fields of view of sensors.) The



Radiometric and Meteorological Instruments are placed at the target site along with electronic power and communication infrastructure.

measurement data are processed by a radiative-transfer computer code to estimate spectral radiances at the position of a sensor known to be overhead at the time of the measurements. These radiances can be compared with the sensor readings to calibrate the sensor.

Previously, in order to perform vicarious calibration, it was necessary to dispatch field teams on expensive measurement campaigns to target sites, scheduled in accordance with sensor overpass times and weather conditions. Difficulty was compounded by remoteness and limited accessibility of typical targets. The present ground facility nearly eliminates the need for field measurement campaigns by acquiring data nearly continuously and making the data available to all interested parties via the World Wide Web.

The present ground facility occupies a target site consisting of the Frenchman Flat dry lakebed located north-northeast of Mercury, Nevada. The instrumentation at the facility includes a light-emitting-diode spectrometer (LSpec), which consists of eight tripod-mounted, ground-viewing radiometer units containing LEDs biased to operate as photodetectors (instead of light emitters) at their respective wavelengths. The LSpec provides an essentially continuous stream of measurements at eight discrete wavelengths. These are merged with spectral surface-reflectance measurements made on occasional site visits to obtain temporally continuous coverage with high spectral resolution. Other equipment at the site includes a weather station

and a tracking sunphotometer (see figure).

Measurement data are acquired at intervals of 5 minutes under all daylight conditions. The data are entered into a database maintained on a Jet Propulsion Laboratory server computer. A remote user can log into a Web-based interface and request information specific to the overpass time of a given sensor. The data can be fed as input to the radiative-transfer computer program to obtain radiances for calibration of the sensor.

*This work was done by Carol Bruegge and Shannon Jackson of Caltech and Mark Helmlinger of Northrop Grumman Space Technology for NASA's Jet Propulsion Laboratory. Further information is contained in a TSP (see page 1).
NPO-45425*

Optical Pressure-Temperature Sensor for a Combustion Chamber

This compact sensor would withstand the harsh combustion environment.

Marshall Space Flight Center, Alabama

A compact sensor for measuring temperature and pressure in a combustion chamber has been proposed. Heretofore, independent measurements of high pressures and temperatures in combustion chambers have not been performed. In the original intended application, the combustion chamber would be that of a rocket engine. Sensors like this one could also be used to measure temperatures and pressures in other combustion chambers and other, similar harsh settings. There could be numerous potential applications in the aeronautical and automotive industries.

In the original rocket-engine application, accurate measurements of pressure and temperature are needed for feedback control to suppress combustion instability. Heretofore, none of the avail-

able pressure sensors have been capable of surviving the thermal environment of a combustion chamber without the use of sensing lines or helium-filled cavities. Pressure-measurement signals obtained by use of sensing lines or helium-filled cavities have altered power spectra that make the signals unsuitable as feedback signals for control purposes.

The proposed sensor would include two optically birefringent, transmissive crystalline wedges: one of sapphire (Al_2O_3) and one of magnesium oxide (MgO), the optical properties of both of which vary with temperature and pressure. The wedges would be separated by a vapor-deposited thin-film transducer, which would be primarily temperature-sensitive (in contradistinction to pressure-sensitive) when attached to a crys-

talline substrate. The sensor would be housed in a rugged probe to survive the extreme temperatures and pressures in a combustion chamber. An externally generated optical input signal would travel through parts of the wedges. The effect of the thin-film transducer on the propagating light beam would provide temperature information. The effect of stress-induced birefringence in the crystalline wedges upon the light beam would provide pressure information.

This work was done by John Wiley of Marshall Space Flight Center, Valentin Korman of Madison Research Corp., and Don Gregory of the University of Alabama in Huntsville. For further information, contact Sammy Nabors, MSFC Commercialization Assistance Lead, at sammy.a.nabors@nasa.gov. Refer to MFS-32075-1.

Impact-Locator Sensor Panels

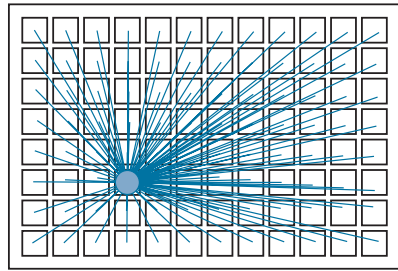
Panels can be electronically daisy-chained and assembled to cover large areas.

Lyndon B. Johnson Space Center, Houston, Texas

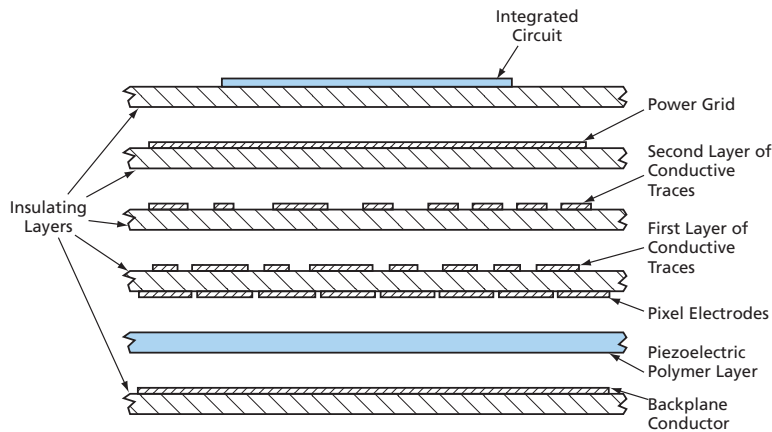
Electronic sensor systems for detecting and locating impacts of rapidly moving particles on spacecraft have been invented. Systems of this type could also be useful on Earth in settings in which the occurrence of impacts and/or the

locations of impacts are not immediately obvious and there are requirements to detect and quickly locate impacts to prevent or minimize damage. For example, occupants of a military vehicle could know immediately that

someone was shooting at it and which side of the vehicle was taking fire. For another example, commercial transportation companies using these systems for remote monitoring of valuable cargo could know when and from what



PLAN VIEW SHOWING PIXELS AND CONDUCTIVE TRACES BETWEEN PIXELS AND INTEGRATED CIRCUIT



MAGNIFIED, EXPLODED CROSS-SECTIONAL VIEW WITH THICKNESSES GREATLY EXAGGERATED AND NOT TO SCALE

A **Typical Sensor Panel** comprises multiple layers of electronic circuitry and a piezoelectric polymer film.

direction impacts were jeopardizing the cargo, whether the impacts were from hailstones, burglary tools, vehicular collisions, or firearms.

The building blocks of a system of this type are sensor panels. Each panel is a thin multilayer structure wherein one of the layers is a commercially available film of poly(vinylidene fluoride) [PVDF], which is a piezoelectric polymer. Because of its piezoelectricity, the film generates an electric potential at the place and time of an impact. Electronic circuitry that is part of the multilayer struc-

ture (as described below) detects this potential, thereby detecting the impact. The panels are constructed identically and can have any convenient dimensions; a width of 16 in. (≈ 0.4 m) and a length of 24 in. (≈ 0.6 m) are typical. Multiple panels can be joined to cover an area as large as required.

The electronic circuitry includes electrodes and conductive traces, on the surfaces of the PVDF film (see figure), that subdivide the panel into pixels within which impacts can be located. Typical pixel dimensions are 2 by 2 in. (about 5

by 5 cm), but pixels could just as well be made larger or smaller as needed. Optionally, the PVDF film could also be scribed into pixels to enhance spatial resolution.

The conductive traces connect the pixel electrodes to an integrated circuit (typically either a field-programmable gate array or an application-specific integrated circuit) on the panel. The integrated circuit detects any impact signals, determines the pixel locations of the signals, determines the pixel location of the first signal, and stores these pixel locations in registers. The integrated circuit then generates a data-transmission word that includes all the pixel impact locations, the first-impact pixel location, and an address unique to the panel. The word is transmitted to an external digital-processor-and-display unit, which could be, for example, a laptop computer. The transmission is fundamentally a notice to the external unit that an impact has been detected at the noted location on the noted panel.

Each panel is connected to external circuits via only two wires, which serve for transmission of both data and power. Wires can be daisy-chained through as many panels as desired, so that only two wires are needed to make the external connections to an assembly of any number of panels. It is not necessary to supply power to operate the piezoelectric transducers; the only power that must be supplied is that required for operation of the integrated circuits on the panels and of the external digital-processor-and-display unit. Hence, the overall power demand of the system is relatively small.

This work was done by Eric L. Christiansen of Johnson Space Center and Terry Byers and Frank Gibbons of Lockheed Martin Corp. Further information is contained in a TSP (see page 1).

This invention is owned by NASA, and a patent application has been filed. Inquiries concerning nonexclusive or exclusive license for its commercial development should be addressed to the Patent Counsel, Johnson Space Center, (281) 483-0837. Refer to MSC-24263-1.



Low-Loss Waveguides for Terahertz Frequencies

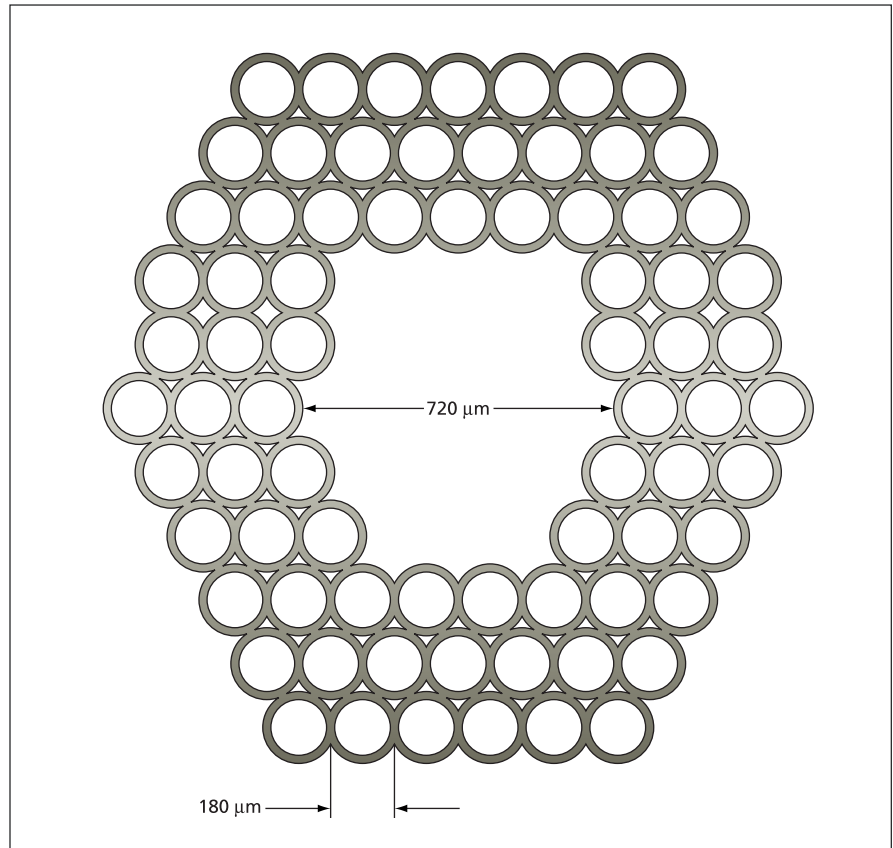
Low-loss, flexible conduits of terahertz power would be developed.

NASA's Jet Propulsion Laboratory, Pasadena, California

Hollow-core, periodic bandgap (HC-PBG) flexible waveguides have been proposed as a means of low-loss transmission of electromagnetic signals in the frequency range from about 300 GHz to 30 THz. This frequency range has been called the "terahertz gap" because it has been little utilized: Heretofore, there has been no way of low-loss guiding of terahertz beams other than by use of fixed-path optical beam guides with lenses and mirrors or multimode waveguides that cannot maintain mode purity around bends or modest discontinuities.

The terahertz HC-PBG waveguide concept utilizes a periodic bandgap structure surrounding a hollow single-mode core to transfer energy with low loss even around bends. The waveguide was developed to enable *in-vivo* applications for THz imaging and sensing at wavelengths from 10 microns to 1 mm, using flexible endoscopes and fiberscopes. Other potential applications include distribution of terahertz power and coupling of signals in general terahertz instrumentation. PBG structures have been developed for a wide range of traveling-wave applications in the microwave and optical regions of the electromagnetic spectrum.

The terahertz HC-PBG waveguide concept involves the same basic physical principles used to optimize infrared PBG structures, but at significantly increased length scales (corresponding to the greater terahertz wavelengths), and with somewhat different geometric arrangements and different materials appropriate to the intended applications. A representative proposed terahertz HC-PBG flexible waveguide (see figure) would comprise a hollow overmoded air or vacuum waveguide core surrounded by a flexible PBG honeycomb structure made of low-loss polyethylene, Teflon, quartz, or high-resistivity silicon tubing. The honeycomb structure would be designed to exhibit bandpass/band-stop behavior for electromagnetic fields of the guided wave penetrating into that structure, resulting



This **Cross Section** of a proposed HC-PBG flexible waveguide shows shapes and sizes optimized for propagation of electromagnetic waves in narrow frequency bands centered around 2.5 THz and 650 GHz — frequencies known to be useful for imaging applications and for which test equipment is available.

in the confinement of the wave within the core for frequencies within one or more desired propagation band(s). Because the core would be hollow and the periodic structure would be of a honeycomb nature, most of the electromagnetic power would propagate in air; therefore, propagation losses would be much lower than that of prior dielectric or metal waveguides.

A major advantage of the proposed structure is flexibility for bending or twisting the waveguide without appreciably distorting the internal electromagnetic fields. In designing this or a similar structure of the same type, the width of the hollow core could be chosen to accommodate insertion of a pyramidal or conical waveguide horn for

exciting the propagating field or coupling the field out to a detector or load.

This work was done by Peter Siegel, Cavour Yeh, Fred Shimabukuro, and Scott Fraser of Caltech for NASA's Jet Propulsion Laboratory.

In accordance with Public Law 96-517, the contractor has elected to retain title to this invention. Inquiries concerning rights for its commercial use should be addressed to:

*Innovative Technology Assets Management
JPL*

*Mail Stop 202-233
4800 Oak Grove Drive
Pasadena, CA 91109-8099
(818) 354-2240*

*E-mail: iaoffice@jpl.nasa.gov
Refer to NPO-41299, volume and number of this NASA Tech Briefs issue, and the page number.*

MEMS/ECD Method for Making $\text{Bi}_{2-x}\text{Sb}_x\text{Te}_3$ Thermoelectric Devices

Devices containing diverse materials in complex three-dimensional shapes can be fabricated.

NASA's Jet Propulsion Laboratory, Pasadena, California

A method of fabricating $\text{Bi}_{2-x}\text{Sb}_x\text{Te}_3$ -based thermoelectric microdevices involves a combination of (1) techniques used previously in the fabrication of integrated circuits and of microelectromechanical systems (MEMS) and (2) a relatively inexpensive MEMS-oriented electrochemical-deposition (ECD) technique. The devices and the method of fabrication at an earlier stage of development were reported in "Submillimeter-Sized $\text{Bi}_{2-x}\text{Sb}_x\text{Te}_3$ Thermoelectric Devices" (NPO-20472), *NASA Tech Briefs*, Vol. 24, No. 5 (May 2000), page 44. To recapitulate: A device of this type generally contains multiple pairs of n- and p-type $\text{Bi}_{2-x}\text{Sb}_x\text{Te}_3$ legs connected in series electrically and in parallel thermally. The $\text{Bi}_{2-x}\text{Sb}_x\text{Te}_3$ legs have typical dimensions of the order of tens of microns. Metal contact pads and other non-thermoelectric parts of the devices are fabricated by conventional integrated-circuit and MEMS fabrication techniques. The $\text{Bi}_{2-x}\text{Sb}_x\text{Te}_3$ thermoelectric legs are formed by electrodeposition, through holes in photoresist masks, onto the contact pads.

Heretofore, most MEMS have been made from materials compatible with silicon integrated-circuit processing, such as silicon, silicon dioxide, and silicon nitride. Moreover, commercial MEMS fabrication techniques have been mostly limited to structures of a substantially two-dimensional character. However, to be useful, thermoelectric microdevices must consist of a variety of materials (including metals and semiconductors), and complex, three-dimensional shapes are needed to effect the required series electrical and parallel thermal connections. In a typical case, the n- and p-type $\text{Bi}_{2-x}\text{Sb}_x\text{Te}_3$ thermoelectric legs must be connected electrically in series with bridging metal interconnections on top and bottom surfaces (see Figure 1). These interconnections are required to be have low contact resistance and high mechanical strength and must be capable of withstanding large current densities and temperature gradients. Most challenging is the requirement to form the p- and n-type tall, heavily doped compound semiconductor legs protruding from the same surface.

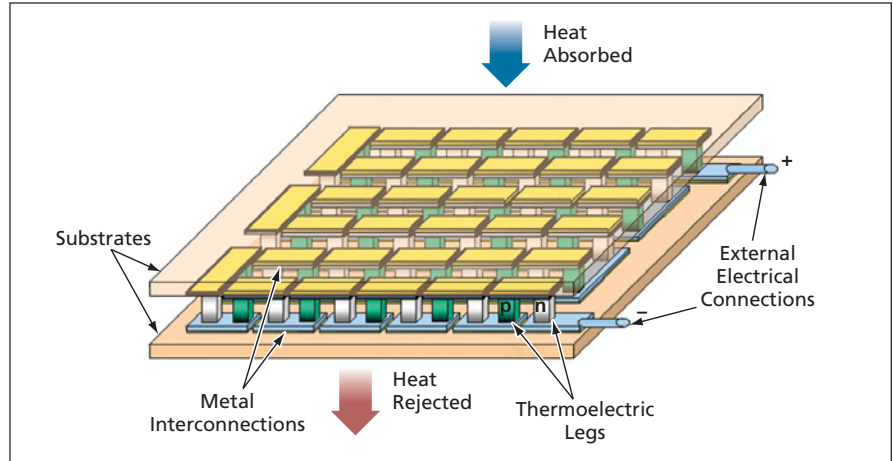


Figure 1. A **Typical Thermoelectric Device** includes multiple n-type and p-type thermoelectric legs sandwiched between two high-thermal-conductivity substrates. The n- and p-type legs are electrically connected in series by alternating top and bottom metal contact pads. Because heat flows from the top to the bottom, all of the thermoelectric legs are thermally connected in parallel. In the cooling mode, an externally applied current forces the heat to flow from the top to the bottom. In the power-generation mode, heat flowing from the top to the bottom drives an electric current through an external load.

The present method overcomes the limitations of prior MEMS fabrication techniques and makes it possible to satisfy the aforementioned requirements. The method is implemented in a process (see Figure 2) that includes the following main steps:

1. In a subprocess that includes sputtering, electrodeposition, photolithography, and etching, a bottom interconnection pattern of Au contact pads (typically $3\ \mu\text{m}$ thick) is formed on a layer of Cr (typically $0.1\ \mu\text{m}$ thick) that has been sputtered onto the oxidized upper surface of an Si substrate.
2. A photoresist having a thickness corresponding to the desired height of the thermoelectric legs is deposited, exposed, and developed to form through-the-thickness holes ending at those portions of the Au contact pads to which the p-type thermoelectric legs are to be bonded.
3. Sb_2Te_3 (p-type) thermoelectric legs are electrodeposited in the holes.
4. A thin layer of photoresist is deposited to cover the tops of the p-type thermoelectric legs.
5. Step 2 is repeated to form holes at the intended locations of Bi_2Te_3 (n-type) thermoelectric legs.
6. The n-type thermoelectric legs are deposited in the holes.

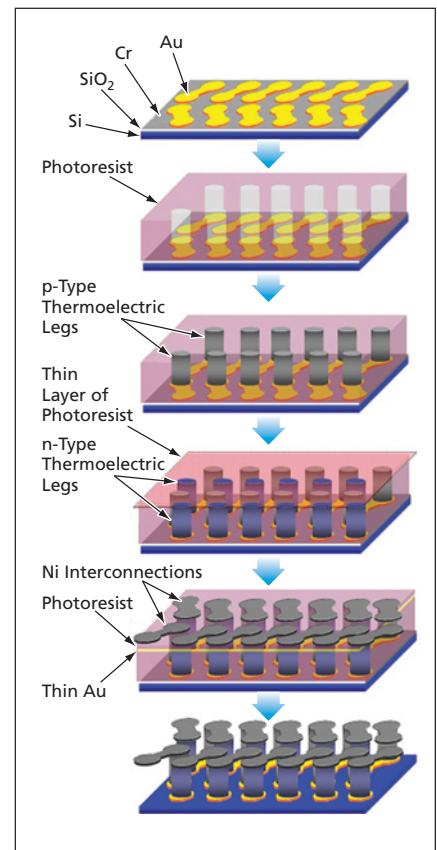


Figure 2. **Metal Interconnections and Thermoelectric Legs** constituting a three-dimensional structure are formed in a multi-step process.

7. The thin top photoresist layer deposited in step 4 is removed.
8. A partly sacrificial layer of gold <0.01 μm thick is deposited to ensure uniform ECD in step 10.
9. A thicker top photoresist layer is deposited and patterned to form a mold for a top interconnection pattern of Ni contact pads.
10. The Ni contact pads, typically 3 μm thick, are electrodeposited in the holes in the mold. The electrodeposition parameters are chosen to keep

stresses in the pads low so that the pads do not pull off the thermoelectric legs.

11. In a series of etches, the excess Cr between the bottom contact pads, the excess Au between the top contact pads, and the photoresist layers are removed.

A device containing 63 Bi_2Te_3 (n-type) and 63 Sb_2Te_3 (p-type) thermoelectric legs, each 20 μm tall and 60 μm in diameter, was fabricated by this method and demonstrated to be capable of thermo-

electric cooling. This device can be considered a prototype of future devices for exerting precise thermal control in microscopic regions and for extracting small amounts of electric power from temperature gradients.

This work was done by James Lim, Chen-Kuo Huang, Margaret Ryan, G. Jeffrey Snyder, Jennifer Herman, and Jean-Pierre Fleurial of Caltech for NASA's Jet Propulsion Laboratory. For further information contact iaoffice@jpl.nasa.gov. NPO-30797

Low-Temperature Supercapacitors

Electrolyte compositions are designed to extend the low-temperature operational limit.

NASA's Jet Propulsion Laboratory, Pasadena, California

An effort to extend the low-temperature operational limit of supercapacitors is currently underway. At present, commercially available non-aqueous supercapacitors are rated for a minimum operating temperature of -40°C . A capability to operate at lower temperatures would be desirable for delivering power to systems that must operate in outer space or in the Polar Regions on Earth.

Supercapacitors (also known as double-layer or electrochemical capacitors) offer a

high power density ($>1,000\text{ W/kg}$) and moderate energy density (about 5 to 10 Wh/kg) technology for storing energy and delivering power. This combination of properties enables delivery of large currents for pulsed applications, or alternatively, smaller currents for low duty cycle applications. The mechanism of storage of electric charge in a supercapacitor — at the electrical double-layer formed at a solid-electrode/liquid-electrolyte interface — differs from that of a primary or secondary electrochemical cell (i.e., a battery) in such a manner as to impart a long cycle life (typically $>10^6$ charge/discharge cycles).

Commercially available non-aqueous supercapacitors are limited in operation to temperatures $\approx -40^\circ\text{C}$ due to the relatively high melting point of the solvent used. Typical electrolytes in commercially available supercapacitors consist of a tetraethylammonium tetrafluoroborate (TEATFB) salt dissolved in one or more solvent(s) that can include acetonitrile [AN (which

freezes at -45.7°C)] and/or propylene carbonate [PC (which freezes at -49°C)]. Moreover, the viscosities of these solvents increase at lower temperatures, with a consequent increase in the equivalent series resistance (ESR) of the supercapacitor cell. This increase in ESR limits the power that can be delivered by the supercapacitor cell at low temperatures.

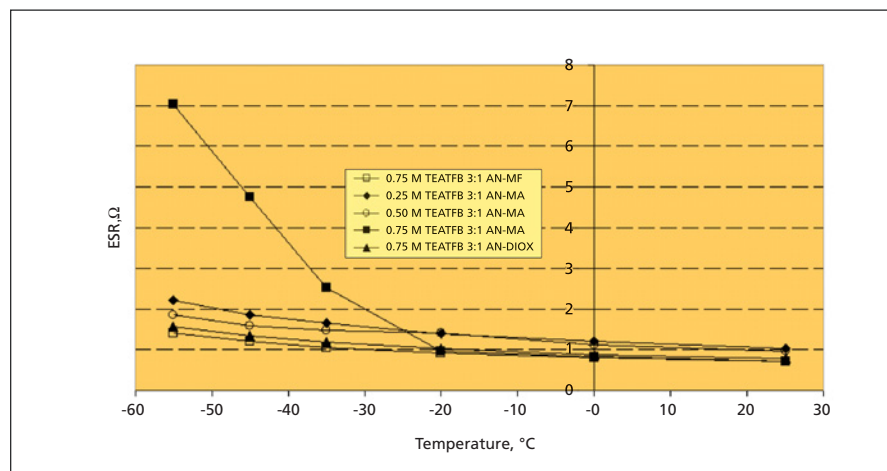
Therefore, efforts to enable operation at lower temperatures have focused on tailoring electrolytes with lower melting points (to extend the temperature range) and higher ionic conductivities and lower viscosities (to minimize increases in ESR). The approach followed thus far has targeted the use of co-solvents to depress the melting point of TEATFB/AN electrolytes while maintaining sufficient solubility of TEATFB at low temperature. These electrolytes are used in conjunction with appropriate electrode materials capable of exhibiting a suitable energy density.

The electrolytes investigated comprise the basic AN/TEATFB formulation in combination with various proportions of co-solvents that include methyl formate, methyl acetate, ethyl acetate, and 1,3-dioxolane (DX) (see table). Coin cells for evaluating the performance of these electrolytes have been fabricated using electrodes made of a commercially available high-surface-area porous carbon-based material. The electrodes were electrically isolated from each other by use of a polyethylene-based separator material. From measurements on these cells, it was concluded that the use of suitable co-solvents can enable retention, at temperatures $< -45^\circ\text{C}$, of room-temperature capacitance values. For one elec-

Co-Solvent	freezing point, $^\circ\text{C}$
ethyl acetate	-72.0
methyl formate	-71.0
methyl acetate	-70.0
1,3-dioxolane*	-67.9
triethylamine	-62.3

* with 2% by volume triethylamine stabilizer

Freezing Point of electrolyte solvent formulations in a 3:1 by volume ratio of acetonitrile to co-solvent.



ESR of Supercapacitor Test Cells is shown down to -55°C , using various low-temperature electrolytes.

trolyte formulation (comprised a 3:1 AN/DX blend), it was found that dc charging and discharging at a temperature as low as -75°C is possible, albeit with capacitance reduced to about half its room-temperature value. By tailoring the nature of the co-solvent and the concentration of the salt used, the ESR can be minimized as well (see figure).

This work was done by Erik J. Brandon, William C. West and Marshall C. Smart of Caltech for NASA's Jet Propulsion Laboratory. Further information is contained in a TSP (see page 1).

In accordance with Public Law 96-517, the contractor has elected to retain title to this invention. Inquiries concerning rights for its commercial use should be addressed to:

*Innovative Technology Assets Management
JPL*

*Mail Stop 202-233
4800 Oak Grove Drive
Pasadena, CA 91109-8099*

*E-mail: iaoffice@jpl.nasa.gov
Refer to NPO-44386, volume and number of this NASA Tech Briefs issue, and the page number.*

Making a Back-Illuminated Imager With Back-Side Contact and Alignment Markers

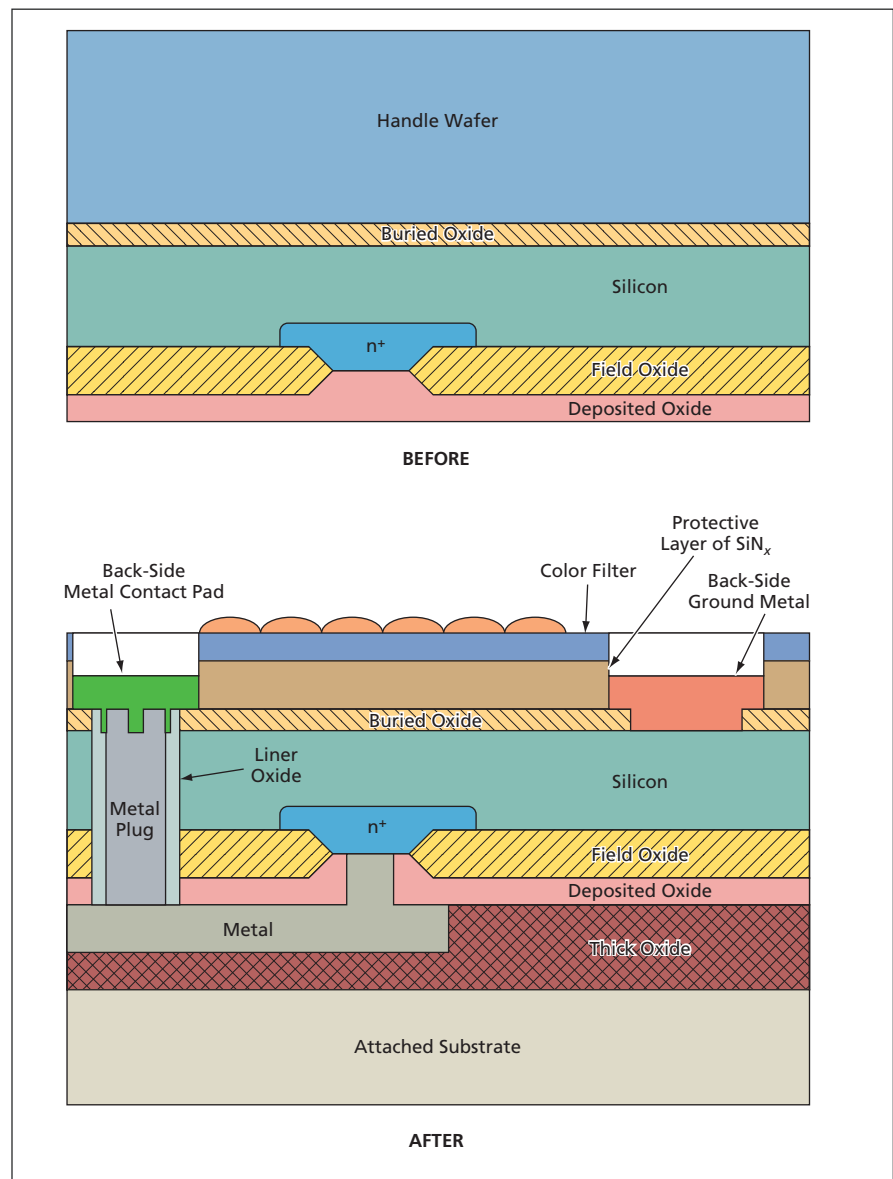
Metal plugs provide both electrical contact and alignment.

NASA's Jet Propulsion Laboratory, Pasadena, California

A design modification and a fabrication process that implements the modification have been conceived to solve two problems encountered in the development of back-illuminated, back-side-thinned complementary metal oxide/semiconductor (CMOS) image-detector integrated circuits. With respect to such an integrated circuit to be fabricated on a silicon substrate, the two problems are (1) how to form metal electrical-contact pads on the back side that are electrically connected through the thickness in proper alignment with electrical contact points on the front side and (2) how to provide alignment keys on the back side to ensure proper registration of back-side optical components (e.g., microlenses and/or color filters) with the front-side pixel pattern. (In this special context, "front side" signifies that face of the substrate upon which the pixel pattern and the associated semiconductor devices and metal conductor lines are formed.)

The essence of the design modification is to add metal plugs that extend from the desired front-side locations through the thickness and protrude from the back side of the substrate. The plugs afford the required front-to-back electrical conduction, and the protrusions of the plugs serve as both the alignment keys and the bases upon which the back-side electrical-contact pads can be formed.

The fabrication process for implementing this design modification would be complex and would be subject to variation as needed for different image-detector applications. Immediately before the beginning of this process, the integrated circuitry would already have been fabricated on the front side of the sub-



These **Simplified Cross Sections** (not to scale) depict the effect of the design modification and process on part of one pixel.

strate, as shown in the upper part of the figure. In terms that are necessarily oversimplified for the sake of brevity, the process can be summarized as follows: Through multiple steps of patterning, etching, and deposition, holes through the substrate would be formed at the desired front-side locations and the metal plugs and their protrusions would be formed in the holes. In subsequent steps, the back-side metal pads would be deposited on the metal plug protrusions, then color filters and/or mi-

cro-lenses would be formed between and in alignment with the metal contact pads, yielding the device structure shown in the lower part of the figure. (Not shown in the figure is a back-side antireflection coat that would be added near the end of the process.)

This work was done by Bedabrata Pain of Caltech for NASA's Jet Propulsion Laboratory. Further information is contained in a TSP (see page 1).

In accordance with Public Law 96-517, the contractor has elected to retain title to

this invention. Inquiries concerning rights for its commercial use should be addressed to:

*Innovative Technology Assets Management
JPL*

*Mail Stop 202-233
4800 Oak Grove Drive
Pasadena, CA 91109-8099
(818) 354-2240*

*E-mail: iaoffice@jpl.nasa.gov
Refer to NPO-42839, volume and number of this NASA Tech Briefs issue, and the page number.*

Compact, Single-Stage MMIC InP HEMT Amplifier

This amplifier exhibits gain of 5 dB at 340 GHz.

NASA's Jet Propulsion Laboratory, Pasadena, California

Figure 1 depicts a monolithic microwave integrated-circuit (MMIC) single-stage amplifier containing an InP-based high-electron-mobility transistor (HEMT) plus coplanar-waveguide (CPW) transmission lines for impedance matching and input and output coupling, all in a highly miniaturized layout as needed for high performance at operating frequencies of hundreds of gigahertz. This is one in a series of devices that are intermediate products of a continuing effort to develop advanced MMIC amplifiers for submillimeter-wavelength imaging systems, scientific instrumentation, heterodyne receivers, and other applications.

The amplifier is designed for operation at a nominal frequency of 340 GHz. The HEMT in this amplifier has a gate length of 35 nm and two fingers each 15 μm wide. The CPWs have a ground-to-ground spacing of only 14 μm . The inclusion of quarter-wavelength-long CPWs for imped-

ance matching and of on-chip shunt capacitors makes it possible to obtain about 5 dB of gain with respectable values of input and output return losses at the design frequency of 340 GHz (see Figure 2). This is among the highest gains per stage at this frequency reported to at the time of this work. Moreover, the measurement data suggest potential for further increase in gain with frequency beyond the 345-GHz limit of the test equipment used to perform the measurements.

This work was done by David Pukala,

Lorene Samoska, King Man Fung, and Todd Gaier of Caltech and W. R. Deal, Gerry Mei, Vesna Radisic, and Richard Lai of Northrop Grumman Corporation for NASA's Jet Propulsion Laboratory. The contributors would like to acknowledge the support of Dr. Mark Rosker and the Army Research Laboratory. This work was supported by the DARPA SWIFT Program and Army Research Laboratory under the DARPA MIPR no.06-U037 and ARL Contract no. W911QX-06-C-0050. Further information is contained in a TSP (see page 1). NPO-44962

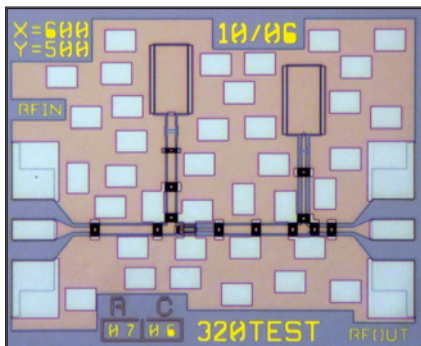


Figure 1. This MMIC Single-Stage Amplifier is a prototype of larger, multistage MMIC amplifiers that will incorporate HEMTs of 35-nm gate length.

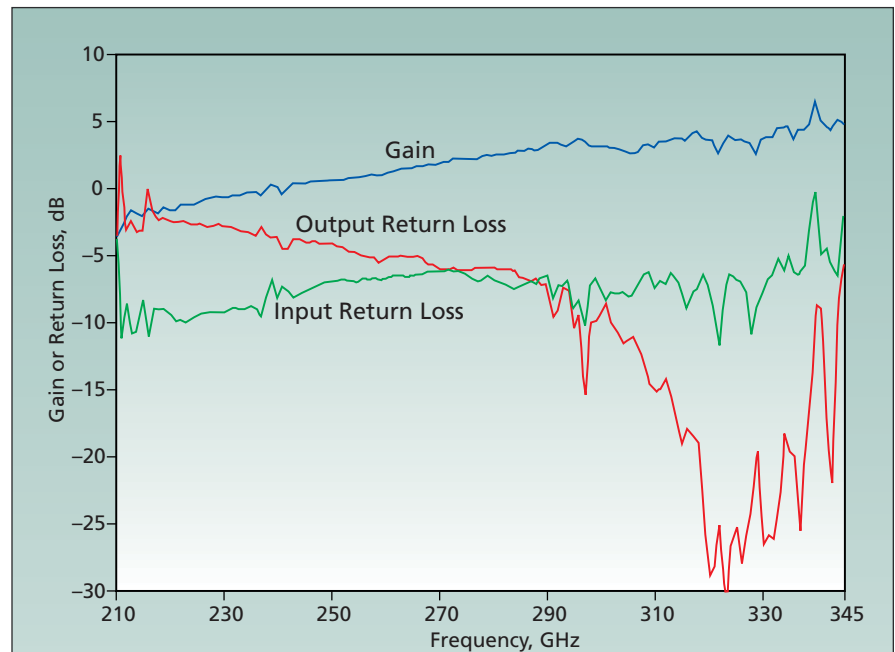


Figure 2. Gain and Input and Output Return Losses of the amplifier of Figure 1 were measured as a function of frequency.

$\text{Nb}_x\text{Ti}_{1-x}\text{N}$ Superconducting-Nanowire Single-Photon Detectors

Potential applications include optical communications and quantum cryptography.

NASA's Jet Propulsion Laboratory, Pasadena, California

Superconducting-nanowire single-photon detectors (SNSPDs) in which $\text{Nb}_x\text{Ti}_{1-x}\text{N}$ (where $x < 1$) films serve as the superconducting materials have shown promise as superior alternatives to previously developed SNSPDs in which NbN films serve as the superconducting materials. SNSPDs have potential utility in optical communications and quantum cryptography.

NbN-based SNSPDs have exhibited, variously, high detection efficiency, low signal jitter, large dynamic range, and low dark counts, but it has been difficult to fabricate detectors that exhibit all of these desirable properties simultaneously. It has been even more difficult to produce NbN-based SNSPDs in high yield, especially in cases in

which the detectors occupy areas larger than 5 by 5 μm .

$\text{Nb}_x\text{Ti}_{1-x}\text{N}$ is a solid solution of NbN and TiN, and has many properties similar to those of NbN. It has been found to be generally easier to stabilize $\text{Nb}_x\text{Ti}_{1-x}\text{N}$ in the high-superconducting-transition-temperature phase than it is to stabilize NbN. In addition, the resistivity and penetration depth of polycrystalline films of $\text{Nb}_x\text{Ti}_{1-x}\text{N}$ have been found to be much smaller than those of films of NbN. These differences have been hypothesized to be attributable to better coupling at grain boundaries within $\text{Nb}_x\text{Ti}_{1-x}\text{N}$ films.

Four batches of prototype $\text{Nb}_x\text{Ti}_{1-x}\text{N}$ SNSPDs fabricated thus far have shown a

yield >60 percent — much higher than the yields of NbN SNSPDs. In two of the batches, the SNSPDs were fabricated in high-resonance-quality-factor (high- Q) cavities by use of commercial dielectric mirrors. The SNSPDs in the high- Q cavities simultaneously exhibited high detection efficiencies, low dark counts, small jitter, and high yield for a resonance wavelength of 1,064 nm. In the most recent two lots fabricated, the yield was high even for large-area (10 by 10 μm) SNSPDs.

This work was done by Jeffrey A. Stern, William H. Farr, Henry G. Leduc, and Bruce Bumble of Caltech for NASA's Jet Propulsion Laboratory. For more information, contact iaoffice@jpl.nasa.gov. NPO-45603



Improved Sand-Compaction Method for Lost-Foam Metal Casting

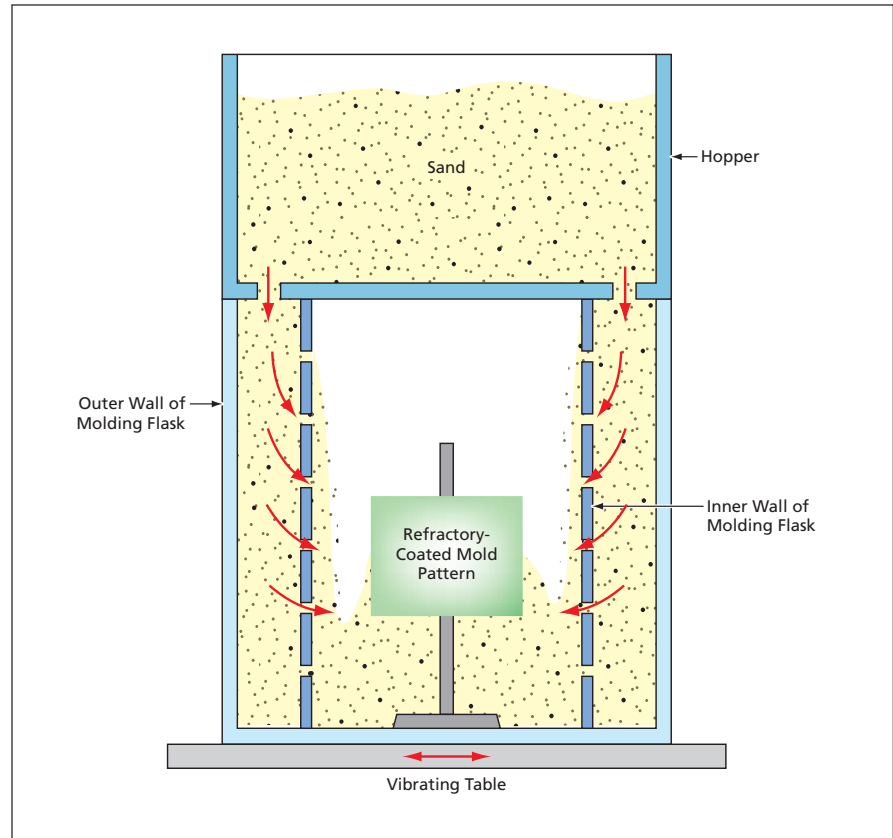
The flow of sand is redirected for better filling and compaction.

Marshall Space Flight Center, Alabama

An improved method of filling a molding flask with sand and compacting the sand around a refractory-coated foam mold pattern has been developed for incorporation into the lost-foam metal-casting process. In comparison with the conventional method of sand filling and compaction, this method affords more nearly complete filling of the space around the refractory-coated foam mold pattern and more thorough compaction of the sand. In so doing, this method enables the sand to better support the refractory coat under metallostatic pressure during filling of the mold with molten metal.

Filling of the molding flask with sand is an important stage in the lost-foam casting process. To obtain a high-quality casting, it is necessary to ensure that the foam mold pattern is surrounded by sand compacted tightly enough so that the sand can support the refractory coat during filling with molten metal. In lost-foam casting as practiced heretofore, the refractory-coated mold pattern is placed in the molding flask and sand is rained from the top until the foam cluster is entirely embedded in sand. During filling with sand, the sand is slightly fluidized, and low-density sand/air mixture is unevenly distributed around the pattern.

To compact the sand around the pattern and to deliver sand into all passages and cavities in the pattern, horizontal and/or vertical vibrations are applied to the flask. However, controlling the motion and maximizing the compaction (and thereby minimizing the permeability) of the sand is a challenging problem. Once the sand particles at lower levels of the flask become interlocked, sand from higher levels cannot be delivered into the pattern cavities at the lower levels. Motion of sand decreases toward the bottom of the sand bed, where compaction has been achieved. If motion and compaction of sand are insufficient, penetration of the refractory coat, and consequent surface defects in the casting, may occur in regions of low compaction. To maintain the desired flow and compaction of sand, some foundries make pauses in the sand rain. However, such pauses increase filling



Sand Flows Sideways into the molding flask, instead of raining down into the flask as in the conventional method.

and compaction time, thereby reducing productivity. The improved method is oriented toward maintaining the desired flow and compaction of sand without introducing pauses in the sand rain.

In the improved method, sand is made to flow into the molding flask substantially horizontally instead of raining down as in the conventional method. For this method, one needs a double-wall molding flask. The outer wall of the flask is solid; the inner wall is perforated with uniformly distributed holes. From a hopper above the flask, sand is supplied to the annular volume between the inner and outer walls. From this annular volume, sand flows horizontally through the holes, into the space surrounding the refractory-coated foam mold pattern (see figure). As in the conventional method,

the flask is vibrated to aid flow and compaction. The motion of sand is more normalized than it is in the conventional method, such that sand is delivered more nearly completely into all passages and cavities, including horizontal passages and inverted pockets. The fluidization of sand is less turbulent than it is in the conventional method. Moreover, compression forces exerted on the mold pattern by raining sand are eliminated — a beneficial effect in that such forces can distort the mold pattern.

This work was done by Sayavur I. Bakhtiyarov and Ruel A. Overfelt of Auburn University for Marshall Space Flight Center. For more information, contact Sammy Nabors, MSFC Commercialization Assistance Lead, at sammy.a.nabors@nasa.gov. MFS-31679-1

Improved Probe for Evaluating Compaction of Mold Sand

Sand is not perturbed during switching among different measurement positions.

Marshall Space Flight Center, Alabama

A nominally stationary tubular probe denoted a telescopic probe has been developed as an improved alternative to a prior movable probe used to evaluate the local degree of compaction of mold sand. The prior movable probe consists mainly of a vertically oriented tube with screen vents at its lower end. The upper end is connected to a source of constant airflow equipped with a pressure gauge. The probe is inserted vertically to a desired depth in a sand-filled molding flask and the back pressure at the given rate of flow of air is recorded as a measure of the degree of partial impermeability and, hence, of the degree of compaction of sand in the vicinity of the probe tip.

Because it is necessary to determine whether sand is adequately compacted at depths throughout the flask, it is necessary to raise or lower the movable probe to place the tip at various depths. Unfortunately, raising or lowering the probe perturbs the sand around the tip, thereby

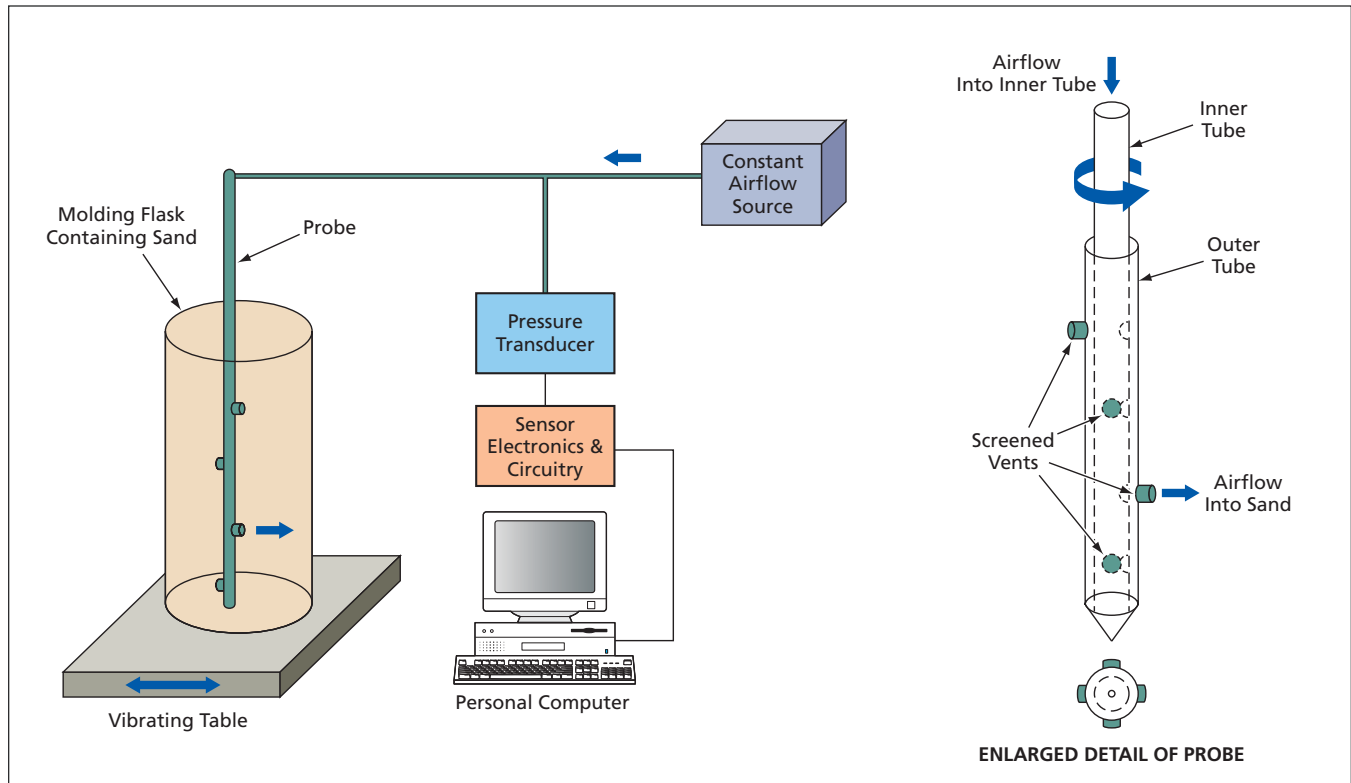
possibly introducing error into the back-pressure reading. Moreover, it can be difficult to raise or lower the probe in well-compacted sand. The design of the telescopic probe overcomes these disadvantages of the movable probe.

The telescopic probe (see figure) includes two concentric circular tubes tightly fitted to each other. There are series of holes along the outer and inner tubes. Screens covering the holes in the outer tube prevent penetration of sand into the probe. Twisting the inner tube relative to the outer tube through a specified angle brings one of the inner-tube holes into alignment with one of the outer-tube holes. The upper end of the inner tube is connected to an airflow-source/back-pressure-measuring apparatus like that of the prior movable probe.

In use, the outer tube of the telescopic probe is mounted in a fixed position in a mold flask and left there as sand is poured into the flask and compacted.

Because the outer tube is not moved during the operations described next, the sand is not perturbed as it is in the case of the movable probe. During pouring and compaction, the inner tube is twisted to prescribed angular positions for aligning inner- and outer-tube holes at corresponding prescribed depths in order to take backpressure readings at those depths. This action is repeated throughout the filling and compaction process to obtain data on backpressure versus depth and time, thereby enabling characterization of the degree of compaction as a function of depth and time.

This work was done by Ruel A. Overfelt of Auburn University and Sayavur I. Bakhtiyarov of New Mexico Institute of Mining & Technology for Marshall Space Flight Center. Inquiries concerning rights for the commercial use of this invention should be addressed to Sammy Nabors, MSFC Commercialization Assistance Lead, at sammy.a.nabors@nasa.gov. Refer to MFS-31678-1.



The Inner Tube Is Rotated to different angles to switch on probe ports at different axial (vertical) positions.



Polymer-Based Composite Catholytes for Li Thin-Film Cells

It should be possible to increase charge capacities and cycle lives.

NASA's Jet Propulsion Laboratory, Pasadena, California

Polymer-based composite catholyte structures have been investigated in a continuing effort to increase the charge/discharge capacities of solid-state lithium thin-film electrochemical cells. A cell according to this concept contains the following layers (see figure):

- An anode current-collecting layer, typically made of Cu;
- An Li metal anode layer;
- A solid electrolyte layer of $\text{Li}_{3.3}\text{PO}_{3.8}\text{N}_{0.22}$ ("LiPON") about 1 to 2 μm thick;
- The aforementioned composite catholyte layer, typically about 100 μm thick, consisting of electronically conductive nanoparticles in an Li-ion-conductive polymer matrix; and
- A metallic cathode current collector, typically made of Mo and about 0.5 μm thick.

In the fabrication of such a cell, the anode current collector (or, alternatively, the Li anode layer if already present as explained in the next paragraph) is first used as a substrate, onto which the

$\text{Li}_{3.3}\text{PO}_{3.8}\text{N}_{0.22}$ layer is deposited. The composite catholyte layer is then cast onto the $\text{Li}_{3.3}\text{PO}_{3.8}\text{N}_{0.22}$ layer. Next, the cathode current collector is deposited on, or pressed into contact with, the composite catholyte layer.

If the anode current collector is a Cu film on a flexible substrate (as in prototype cells) or if it is something similar, the Li anode layer can be formed by plating of Li on the anode current collector during the first charge. Alternatively, the anode layer can be made, at the outset, of a thin film of Li; if this were done, the cell could retain a greater fraction of its capacity over many cycles because the film could be made to contain a slight excess of Li that would be available to replace some Li that is lost to the surroundings during cycling.

Inasmuch as $\text{Li}_{3.3}\text{PO}_{3.8}\text{N}_{0.22}$ is an amorphous, flexible material, the cell as a whole can be a free-standing, flexible structure. Theoretically, the capacity of the cell can

equal or perhaps exceed that of a typical state-of-the-art lithium thin-film cell. The inclusion of the $\text{Li}_{3.3}\text{PO}_{3.8}\text{N}_{0.22}$ is expected to result in extended lifetime and enables the use of Li in metallic form because the hazards associated with the combination of metallic Li and liquid electrolyte are not present. Further, it is anticipated that the cell would have long (relative to prior Li thin-film cells) cycle life at temperature up to 150 °C, provided that the proper cathode material is selected.

The capacities of the prototype cells thus far have been below theoretically attainable values. It seems likely that the theoretical values could be approached by selecting the proper cathode material and including thin Li anode films at the outset.

This work was done by Jay Whitacre, William West, Keith Chin, and Sekharipuram Narayanan of Caltech for NASA's Jet Propulsion Laboratory. Further information is contained in a TSP (see page 1).

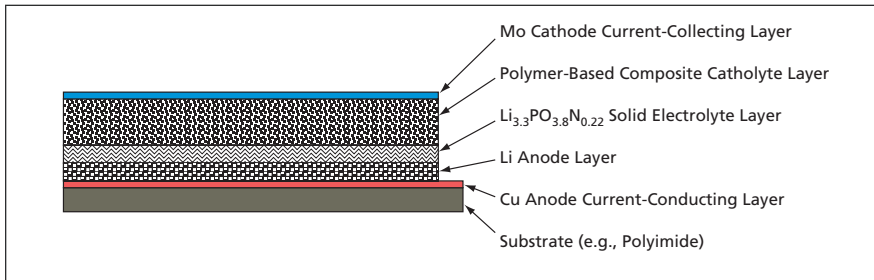
In accordance with Public Law 96-517, the contractor has elected to retain title to this invention. Inquiries concerning rights for its commercial use should be addressed to:

*Innovative Technology Assets Management
JPL*

*Mail Stop 202-233
4800 Oak Grove Drive
Pasadena, CA 91109-8099
(818) 354-2240*

E-mail: iaoffice@jpl.nasa.gov

Refer to NPO-41068, volume and number of this NASA Tech Briefs issue, and the page number.



A Polymer-Based Composite Catholyte Layer may be the key to high charge/discharge capacity in an Li thin-film cell. In prototype cells, the catholyte layers consisted of LiCoO_2 , polyethylene oxide, lithium trifluoromethanesulfonate, and carbon black.

Using ALD To Bond CNTs to Substrates and Matrices

CNT-based field emitters could be made more durable.

NASA's Jet Propulsion Laboratory, Pasadena, California

Atomic-layer deposition (ALD) has been shown to be effective as a means of coating carbon nanotubes (CNTs) with layers of Al_2O_3 that form strong bonds between the CNTs and the substrates on which the CNTs are grown. It should also be possible to form strong

CNT/substrate bonds using other coating materials that are amenable to ALD — for example, HfO_2 , Ti, or Ta. Further, it has been conjectured that bonds between CNTs and matrices in CNT/matrix composite materials could be strengthened by ALD of suitable coat-

ing materials on the CNTs.

The need to increase adhesion between CNTs and substrates on which they are grown was noticed in examination of prototype advanced field emitters consisting of arrays of vertically aligned bundles of CNTs grown on iron

catalyst dots on silicon substrates: It was found that the CNTs are easily peeled off the substrates by abrasion or by pulling with adhesive tape and that the CNTs might also be pulled off the substrates by application of strong electric fields.

ALD is a previously developed vapor-phase thin-film-growth technique. The full name of the technique reflects the fact that it is possible to tailor the film thickness to a precision of the order of a single layer of deposited atoms and, thus, to form a highly uniform, conformal coating. ALD differs from conventional chemical vapor deposition, in which material is deposited continually by thermal decomposition of a precursor gas. In ALD, material is deposited one layer of atoms at a time because the deposition process is self-limiting and driven by chemical reactions between the precursor gas and the surface of the substrate or the previously deposited layer. In order to enable growth of the next layer, it is necessary to first effect an activation subprocess that imparts the needed chemical reactivity to the surface. Thus, the thickness of the deposit can be tailored by

simply choosing the number of activation/growth cycles.

The use of ALD for coating CNTs to increase adhesion was demonstrated in experiments on specimens comprising multiwalled CNTs grown to lengths of hundreds of microns extending away from 2.5-nm-thick iron catalyst layers on silicon substrates. The CNTs were coated with Al_2O_3 by ALD using trimethoxyaluminum and water vapor as precursor gases at a growth temperature of 250 °C. The Al_2O_3 was deposited to a thickness of 170 nm in 1,700 activation/growth cycles. Preparation of the specimen surfaces prior to ALD was found to be necessary for the success of the ALD: Specifically, it was found to be necessary to heat the specimens in air at a temperature of 500 °C to increase the density of hydroxyl groups on the substrate and CNT surfaces that enable formation of covalent bonds with the Al_2O_3 deposits. In the absence of such preparation, the Al_2O_3 deposits separated from the substrate surfaces.

The adhesion strengths of the ALD-coated CNTs were quantified by pull tests using known weights. For example,

in the case of one specimen containing an array comprising 5- μm -diameter bundles of CNTs separated by 5- μm gaps, the measured adhesion strength was 1.23 MPa. It should be noted that this measurement sets a lower bound inasmuch as the strength value was calculated by dividing the applied force by the specimen area. After accounting for the fact that the entire specimen area was not covered by CNTs, the adhesion strength was estimated to be >10 MPa.

This work was done by Eric W. Wong, Michael J. Bronikowski, and Robert S. Kowalczyk of Caltech for NASA's Jet Propulsion Laboratory.

In accordance with Public Law 96-517, the contractor has elected to retain title to this invention. Inquiries concerning rights for its commercial use should be addressed to:

*Innovative Technology Assets Management
JPL*

*Mail Stop 202-233
4800 Oak Grove Drive
Pasadena, CA 91109-8099*

E-mail: iaoffice@jpl.nasa.gov

Refer to NPO-45403, volume and number of this NASA Tech Briefs issue, and the page number.

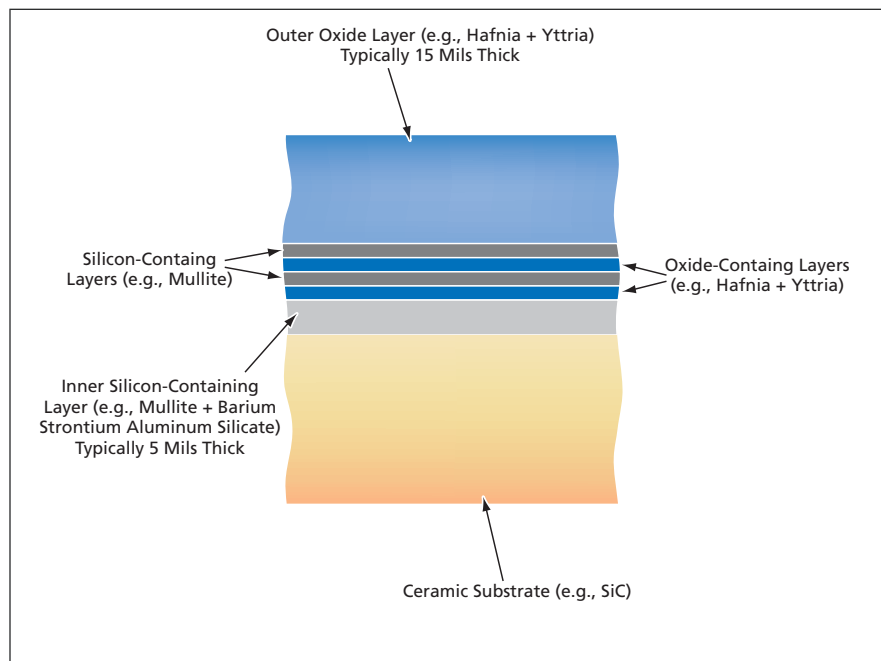
Alternating-Composition Layered Ceramic Barrier Coatings

These coatings are expected to be more durable, relative to prior thermal/environmental barrier coatings.

John H. Glenn Research Center, Cleveland, Ohio

Ceramic thermal and environmental barrier coatings (T/EBCs) that contain multiple layers of alternating chemical composition have been developed as improved means of protecting underlying components of gas-turbine and other heat engines against both corrosive combustion gases and high temperatures. A coating of this type (see figure) is configured using the following layers:

- An outer, or top oxide layer that has a relatively high coefficient of thermal expansion (CTE) and serves primarily to thermally protect the underlying coating layers and the low-CTE ceramic substrate structural material (the component that is ultimately meant to be protected) from damage due to exposure at the high temperatures to be experienced in the application;
- An inner, or bottom silicon-containing/silicate layer, which is in contact with the substrate, has a low CTE and



Alternating-Composition Intermediate Layers dissipate strain energy arising from the thermal-expansion mismatch between the inner and outer coating layers.

serves primarily to keep environmental gases away from the substrate; and

- Multiple intermediate layers of alternating chemical composition (and, hence, alternating CTE).

The intermediate alternating-composition coating layers are chemically compatible with themselves as well as with the inner and outer coating layers. These intermediate coating layers act as an energy-dissipating interlayer: they dissipate strain energy associated with the CTE mismatch between the inner and outer coating layers, thereby reducing stresses and helping to increase (relative to prior ceramic T/EBCs) coating resistance to cracking and delamination from the substrate surface.

Typically, there are between four and ten alternating-composition intermediate layers, comprising higher-CTE oxide layers interspersed with lower-CTE silicate layers, each layer having a thickness between 5 and 50 μm . The compositions of the oxide and silicate alternating layers can be the same as those of the outer and inner layers, respectively. Alternatively, different oxide and silicate compositions

can be chosen to increase tolerance of strain, resistance to cracking, and/or protection against chemical attack by gases in any intended application.

During thermal cycling, the alternating layers become regions of alternating tension and compression. This stress and strain configuration facilitates microsegmentation in the oxide layers while maintaining effective compression in the silicate layers. As a consequence, the thermal expansion of the energy-dissipating interlayer is reduced, stresses are reduced, and tolerance of strain is greatly enhanced. Cracking that starts in the outer oxide layer of the coating is arrested within the alternating layers because of the compressive stress in the silicate alternating layers and the tendency toward deflection and/or bifurcation of cracks at the interfaces between the alternating layers. Moreover, during cooling, the compression in the silicate alternating layers helps to ensure the integrity of the overall coating system in its role as an environmental barrier by helping to prevent penetration of combustion gases to the surface of the substrate.

The thickness of the alternating oxide and silicate layers are quite dependent on the intended engine application. A thicker-silicate-layer/thinner-oxide-layer structure could increase the strain tolerance of the coating and protect the substrate (or engine component in application) from the hot gases in the engine environment; however, on the other hand, a slightly thinner silicate-layer next to a slightly thicker oxide-layer structure could increase the coating's resistance to stress and penetration of any damaging gas-constituents through cracks, potentially reacting with the substrate.

This work was done by Robert A. Miller of Glenn Research Center and Dongming Zhu of the U. S. Army Research Laboratory. Further information is contained in a TSP (see page 1).

Inquiries concerning rights for the commercial use of this invention should be addressed to NASA Glenn Research Center, Innovative Partnerships Office, Attn: Steve Fedor, Mail Stop 4-8, 21000 Brookpark Road, Cleveland, Ohio 44135. Refer to LEW-17536-1.



Variable-Structure Control of a Model Glider Airplane

The conventional spin-recovery technique for fuselage-heavy aircraft is implemented by a modern control system.

Langley Research Center, Hampton, Virginia

A variable-structure control system designed to enable a fuselage-heavy airplane to recover from spin has been demonstrated in a hand-launched, instrumented model glider airplane (see figure). It has long been known that the most effective spin recovery technique for fuselage-heavy aircraft involves the use of ailerons to roll the airplane into the spin. This technique might be considered counter-intuitive because the pro-spin aileron deflection tends to ini-



This Model Glider Airplane, instrumented with sensors and control and data-acquisition systems, was used to demonstrate the use of variable-structure control for spin recovery.

tially increase the roll-rate component of the angular momentum of the airplane. However, it restores some controllability, enabling the pilot to perform subsequent maneuvers to pull out of the spin. The design of the present model-airplane control system was inspired in part by recognition that the aforementioned (and conventional) spin-recovery technique mimics a variable-structure control law.

Variable-structure control is a high-speed switching feedback control technique that has been developed for control of nonlinear dynamic systems. A variable-structure control law typically has two phases of operation, denoted the reaching-mode and sliding-mode phases. In the reaching-mode phase, a nonlinear relay control strategy is followed to drive the trajectory of the system to a pre-defined switching surface within the motion state space. The sliding-mode phase involves motion along the switching surface as the system moves toward an equilibrium or critical point.

A theoretical analysis has led to the conclusion that the conventional spin-recovery technique can be interpreted as a variable-structure control law with a switching surface defined at zero yaw rate. Application of Lyapunov stability

methods in the theoretical analysis showed that deflecting the ailerons in the direction of the spin helps to insure that this switching surface is stable. It was shown that during the reaching-mode phase, a simple relay control law would drive the airplane to a critical point that would be characterized by almost pure rolling motion. The sliding-mode-phase control law would then eliminate the rolling motion, leading to a complete recovery.

For the demonstration of variable-structure control for spin recovery, the model airplane was equipped with attitude sensors and a microcontroller that drove servomechanisms for controlling the deflections of the ailerons, rudder, and elevator. A variable-structure control law incorporating a nonlinear model of the aerodynamic characteristics of the airplane was implemented in firmware. Flight tests have verified the stability of the reaching-mode phase.

This work was done by Martin R. Waszak of Langley Research Center and Mark R. Anderson of Paper Pilot Research, Inc. Further information is contained in a TSP (see page 1). LAR-17106-1

Axial Halbach Magnetic Bearings

Complex active control systems are not needed.

John H. Glenn Research Center, Cleveland, Ohio

Axial Halbach magnetic bearings have been investigated as part of an effort to develop increasingly reliable noncontact bearings for future high-speed rotary machines that may be used in such applications as aircraft, industrial, and land-vehicle power systems and in some medical and scientific instrumentation systems. Axial Halbach magnetic bearings are passive in the sense that unlike

most other magnetic bearings that have been developed in recent years, they effect stable magnetic levitation without need for complex active control.

In simplest terms, the basic principle of levitation in an axial Halbach magnetic bearing is that of the repulsive electromagnetic force between (1) a moving permanent magnet and (2) an electric current induced in a stationary

electrical conductor by the motion of the magnetic field. An axial Halbach bearing includes multiple permanent magnets arranged in a Halbach array ("Halbach array" is defined below) in a rotor and multiple conductors in the form of wire coils in a stator, all arranged so the rotary motion produces an axial repulsion that is sufficient to levitate the rotor.

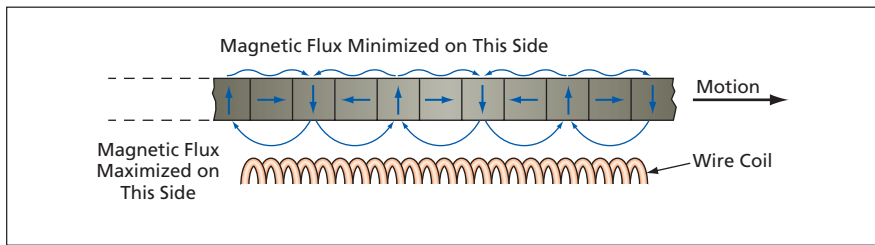


Figure 1. A **Basic Halbach Array** consists of permanent magnets oriented in a sequence of quarter turns chosen to concentrate the magnetic field on one side. The motion of the array along a wire coil gives rise to an electromagnetic repulsion that can be exploited for levitation.

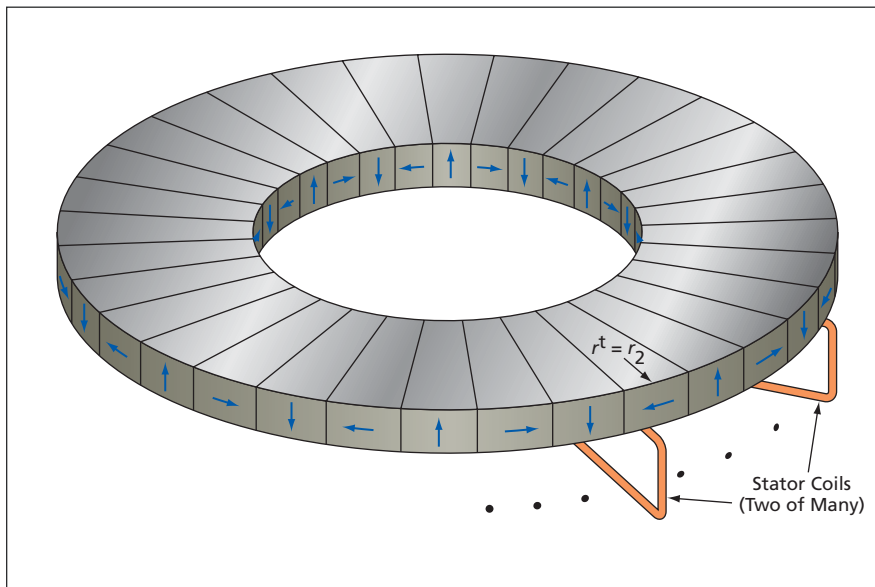


Figure 2. An **Axial Halbach Magnetic Bearing** includes a symmetrical disk version of the Halbach array of Figure 1 plus multiple stator coils in a symmetrical array below the magnet disk. For simplicity, only two of the stator coils are shown.

A basic Halbach array (see Figure 1) consists of a row of permanent magnets, each oriented so that its magnetic field is at a right angle to that of the adjacent magnet, and the right-angle turns are sequenced so as to maximize the magnitude of the magnetic flux density on one side of the row while minimizing it on

the opposite side. The advantage of this configuration is that it makes it possible to approach the theoretical maximum force per unit area that could be exerted by a given amount of permanent-magnet material. The configuration is named after physicist Klaus Halbach, who conceived it for use in particle accelerators.

Halbach arrays have also been studied for use in magnetic-levitation (“maglev”) railroad trains.

In an axial Halbach magnetic bearing, the basic Halbach arrangement is modified into a symmetrical arrangement of sector-shaped permanent magnets in a disk on the rotor (see Figure 2). The magnets are oriented to concentrate the magnetic field on one of the axial faces of the disk — the lower face in Figure 2. The stator coils are mounted in a symmetrical arrangement below the disk.

At a given radial and axial coordinate relative to the disk, the magnetic flux along any given direction varies approximately sinusoidally with the azimuthal angular coordinate. When the disk rotates, the temporal variation of the magnetic field intercepted by the stator coils induces electric currents, thereby generating a repulsive electromagnetic force. The circuits of the stator coils may be terminated with external inductors, the values of which are chosen to modify the phase shifts of voltage and currents so as to maximize the axial repulsion. At and above a critical speed that depends on the specific design, the repulsive force is sufficient to levitate the rotor. During startup, shutdown, and other events in which the rate of rotation falls below the critical speed, the rotor comes to rest on an auxiliary mechanical bearing.

This work was done by Dennis J. Eichenberg, Christopher A. Gallo, and William K. Thompson of Glenn Research Center. Further information is contained in a TSP (see page 1).

Inquiries concerning rights for the commercial use of this invention should be addressed to NASA Glenn Research Center, Innovative Partnerships Office, Attn: Steve Fedor, Mail Stop 4-8, 21000 Brookpark Road, Cleveland, Ohio 44135. Refer to LEW-18066-1.

✿ Compact, Non-Pneumatic Rock-Powder Samplers

Tool bits for ultrasonic/sonic drill/corers are modified to trap small particles.

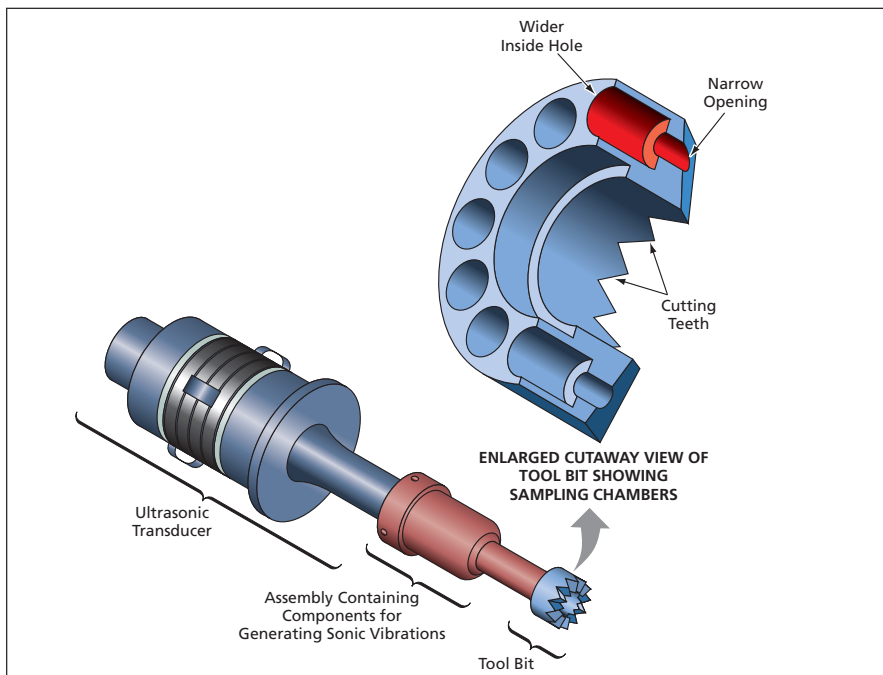
NASA’s Jet Propulsion Laboratory, Pasadena, California

Tool bits that automatically collect powdered rock, permafrost, or other hard material generated in repeated hammering action have been invented. These tool bits are intended primarily for use as parts of ultrasonic/sonic drill corers (USDCs) and related apparatuses, which have been reported in numerous prior *NASA Tech Briefs* articles. A USDC is based on the concept of a

miniature, lightweight, low-power, piezoelectrically driven hammering mechanism that is excited with a combination of ultrasonic and sonic vibrations that enable its tool bit to bore into rock or other hard, brittle material with very little applied force. There are numerous potential applications for such apparatuses in geological exploration on Earth and on remote planets. Typi-

cally, in such an exploration, the purpose served by a USDC is to cut samples of fragmented rock from one or more depth(s).

The present invention pertains to the special case in which it is desired to collect samples in powder form for analysis by x-ray diffraction and possibly other techniques. In one prior approach, rock fragments generated by a USDC or



Sampling Chambers consisting of narrow openings leading to wider inside holes are incorporated into the tool bit of an ultrasonic/sonic drill corer.

other apparatus were first collected by some independent means, then placed into a chamber in the same or a different USDC or USDC-like apparatus, wherein the fragments were crushed into powder. In another prior approach, powder generated at the cutting face of a USDC tool bit was blown into a collec-

tion chamber by a pulse of pressurized gas. The present invention eliminates the need for both the mechanical collection equipment and the crushing chamber of the first-mentioned prior approach and the pneumatic collection equipment of the second-mentioned prior approach, so that it becomes possi-

ble to make the overall sample-acquisition apparatus more compact.

A tool bit according to the present invention (see figure) is hollow and includes holes at or near its cutting tip. Some of the powder kicked up during cutting enters the interior of the tool through the holes. To make the tool more effective in trapping the powder that enters, the holes are tapered (e.g., stepped as in the figure, or else conical), with narrow openings leading to wider inside holes. The narrow openings prevent the entry of wider rock fragments. The collected powder is retained in the tool until needed for analysis. To dispense the powder for analysis, the USDC actuator is simply turned on to shake the powder out through the holes into a suitable receptacle. Experiments have shown that the powdered rock generated by use of a tool bit of this type has essentially the same particle-size distribution, suitable for x-ray diffraction studies, as does powdered rock generated by a commercially available laboratory rock-crushing mill.

This work was done by Stewart Sherrit, Yoseph Bar-Cohen, Mircea Badescu, Xiaoqi Bao, Zensheu Chang, Christopher Jones, and Jack Aldrich of Caltech for NASA's Jet Propulsion Laboratory. For more information, contact iaoffice@jpl.nasa.gov. NPO-43614



Biochips Containing Arrays of Carbon-Nanotube Electrodes

Small quantities of biomarkers could be detected rapidly, with simplified preparation.

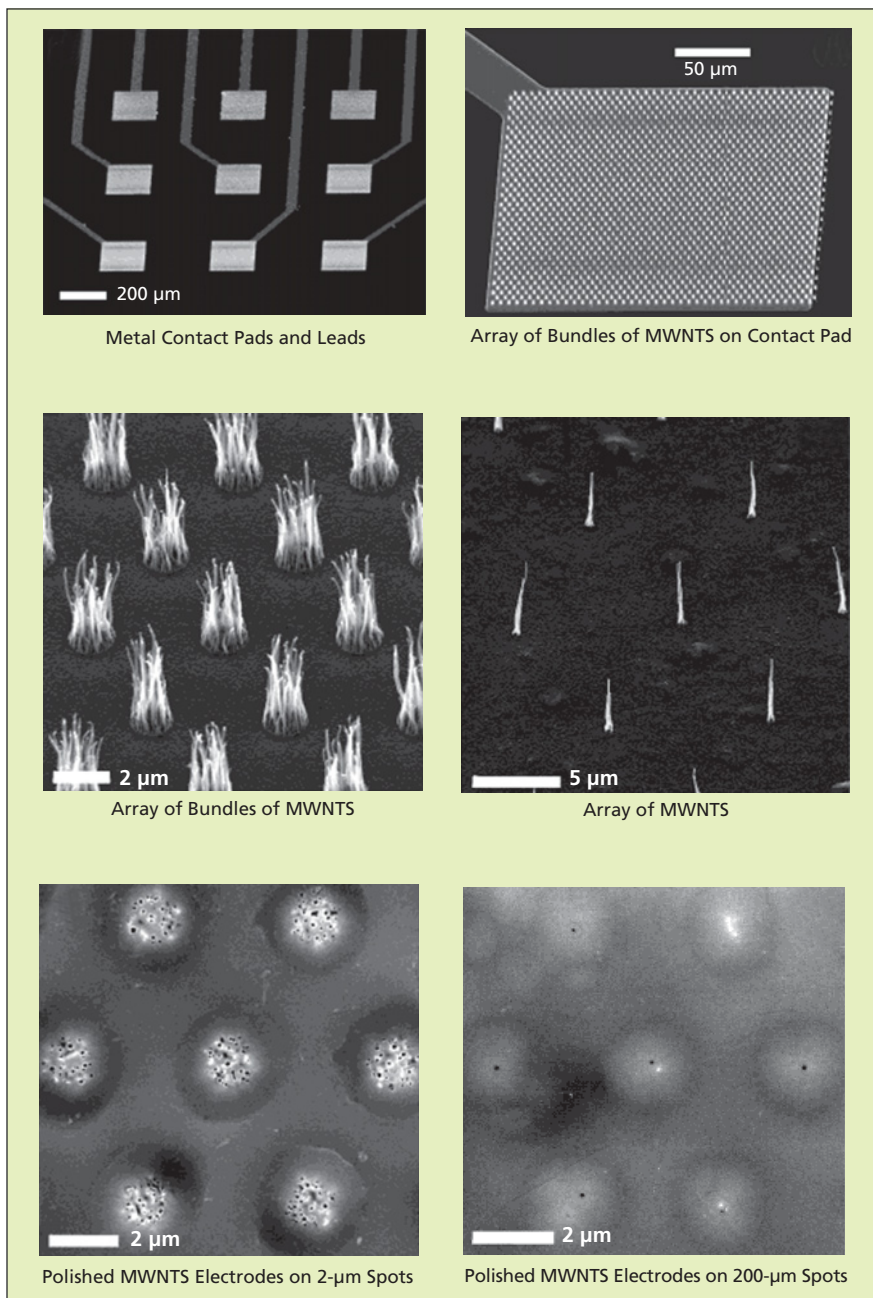
Ames Research Center, Moffett Field, California

Biochips containing arrays of nano-electrodes based on multiwalled carbon nanotubes (MWCNTs) are being developed as means of ultrasensitive electrochemical detection of specific deoxyribonucleic acid (DNA) and messenger ribonucleic acid (mRNA) biomarkers for purposes of medical diagnosis and bioenvironmental monitoring. In mass production, these biochips could be relatively inexpensive (hence, disposable). These biochips would be integrated with computer-controlled microfluidic and microelectronic devices in automated hand-held and bench-top instruments that could be used to perform rapid *in vitro* genetic analyses with simplified preparation of samples.

Carbon nanotubes are attractive for use as nanoelectrodes for detection of biomolecules because of their nanoscale dimensions and their chemical properties.

- In general, as the size of an electrode is reduced, the signal-to-noise ratio (hence, the sensitivity) and the temporal resolution obtainable in the use of the electrode increase. Of course, the nanoscale dimensions of carbon nanotubes are favorable for miniaturization.
- MWCNTs having large length-to-diameter ratios, standing on metal contact pads, can readily be fabricated at wafer scale to form well-defined nanoelectrode arrays.
- MWCNTs have a wide potential window and well-defined surface functional groups, and have a high degree of biocompatibility — properties that are attractive for biosensor applications.

A biochip according to this concept includes a planar array of metal electrode contact pads and leads embedded in a dielectric substrate that typically consists of SiO₂. A single MWCNT, a bundle of MWCNTs, or an array of single MWCNTs or bundles thereof oriented perpendicular to the plane is attached to each contact pad and is long enough to lie flush with (or protrude slightly from) the outer surface of the dielectric (see figure). The exposed tips of



These **Electron Micrographs** are representative of experimental nanoelectrode-array biochips at various stages of fabrication.

the MWCNTs are covalently functionalized with such biomolecular probe substances as oligonucleotides, peptides, proteins, ligands, and/or enzymes cho-

sen to interact with specific target biomolecules. In a typical envisioned application, the binding of the target molecules with the probe molecules and/or

the products of enzyme-catalyzed chemical reactions would be detected by electrochemical methods. It is important to emphasize that unlike in some prior detection methods, time-consuming fluorescence labeling of target DNA would be unnecessary because the electrochemical signals associated with the bound target molecules can be directly electronically measured.

The fabrication of a biochip containing such an array of functionalized nanoelectrodes begins with the prefabrication of the metal electrode contact pads and leads on a SiO₂ covered silicon substrate. The MWCNTs are formed on the prefabricated contact pads by wafer-scale plasma enhanced chemical vapor deposi-

tion. In a second chemical-vapor-deposition process, the contact pads and the MWCNTs are encapsulated in SiO₂. Then by chemical mechanical polishing, SiO₂ is removed to a depth sufficient to form a planar SiO₂ outer surface with the exposed tips of the MWCNTs constituting an array of inlaid nanodisk electrodes.

In development work thus far, electrical and electrochemical properties of embedded arrays of MWCNT nanoelectrodes have been thoroughly characterized. Nanoelectrodes have been covalently functionalized with probe molecules through formation of amide bonds at exposed end of MWCNTs. Direct electrochemical detection of oxidation signals of inherent guanine bases in

target nucleic acids has been demonstrated. It has been shown that fewer than 1,000 DNA or mRNA targets for each biomarker can be directly detected, making it possible to measure mRNA without amplification by polymerase chain reaction.

This work was done by Jun Li, M. Meyyappan, and Jessica Koehne of Ames Research Center, Alan Cassell of UASRC, and Hua Chen of ELORET Corp. Further information is contained in a TSP (see page 1).

This invention is owned by NASA and a patent application has been filed. Inquiries concerning rights for the commercial use of this invention should be addressed to the Ames Technology Partnerships Division at (650) 604-2954. Refer to ARC-15205-1.



⊗ $Nb_xTi_{1-x}N$ Superconducting-Nanowire Single-Photon Detectors

Potential applications include optical communications and quantum cryptography.

NASA's Jet Propulsion Laboratory, Pasadena, California

Superconducting-nanowire single-photon detectors (SNSPDs) in which $Nb_xTi_{1-x}N$ (where $x < 1$) films serve as the superconducting materials have shown promise as superior alternatives to previously developed SNSPDs in which NbN films serve as the superconducting materials. SNSPDs have potential utility in optical communications and quantum cryptography.

NbN-based SNSPDs have exhibited, variously, high detection efficiency, low signal jitter, large dynamic range, and low dark counts, but it has been difficult to fabricate detectors that exhibit all of these desirable properties simultaneously. It has been even more difficult to produce NbN-based SNSPDs in high yield, especially in

cases in which the detectors occupy areas larger than 5 by 5 μm .

$Nb_xTi_{1-x}N$ is a solid solution of NbN and TiN, and has many properties similar to those of NbN. It has been found to be generally easier to stabilize $Nb_xTi_{1-x}N$ in the high-superconducting-transition-temperature phase than it is to stabilize NbN. In addition, the resistivity and penetration depth of polycrystalline films of $Nb_xTi_{1-x}N$ have been found to be much smaller than those of films of NbN. These differences have been hypothesized to be attributable to better coupling at grain boundaries within $Nb_xTi_{1-x}N$ films.

Four batches of prototype $Nb_xTi_{1-x}N$ SNSPDs fabricated thus far have shown a

yield >60 percent — much higher than the yields of NbN SNSPDs. In two of the batches, the SNSPDs were fabricated in high-resonance-quality-factor (high- Q) cavities by use of commercial dielectric mirrors. The SNSPDs in the high- Q cavities simultaneously exhibited high detection efficiencies, low dark counts, small jitter, and high yield for a resonance wavelength of 1,064 nm. In the most recent two lots fabricated, the yield was high even for large-area (10 by 10 μm) SNSPDs.

This work was done by Jeffrey A. Stern, William H. Farr, Henry G. Leduc, and Bruce Bumble of Caltech for NASA's Jet Propulsion Laboratory. For more information, contact iaoffice@jpl.nasa.gov. NPO-45603

⊗ Neon as a Buffer Gas for a Mercury-Ion Clock

NASA's Jet Propulsion Laboratory, Pasadena, California

One aspect of the topic of "Compact, Highly Stable Ion Clock" (NPO-43075), *NASA Tech Briefs*, Vol. 32, No. 5 (May 2008), page 63, is examined in more detail. To recapitulate: A developmental miniature mercury-ion clock has stability comparable to that of a hydrogen-maser clock. The ion-handling components are housed in a sealed vacuum tube, wherein a getter pump is used to maintain the partial vacuum, and the evacuated tube is backfilled

with mercury vapor in a buffer gas.

The development has included a study of gas-induced shifts of the clock frequency and of alternatives to the traditional use of helium as the buffer gas. The frequency-shifting effects of three inert gases (helium, neon, and argon) and three getterable gases (hydrogen, nitrogen, and methane) were measured. Neon was determined to be the best choice for the buffer gas: The pressure-induced frequency pulling by

neon was found to be only about two-fifths of that of helium. Furthermore, because neon diffuses through solids much more slowly than does helium, the operational lifetime of a tube back-filled with neon could be considerably longer than that of a tube backfilled with helium.

This work was done by John Prestage and Sang Chung of Caltech for NASA's Jet Propulsion Laboratory. For more information, contact iaoffice@jpl.nasa.gov. NPO-42919

⊗ Miniature Incandescent Lamps as Fiber-Optic Light Sources

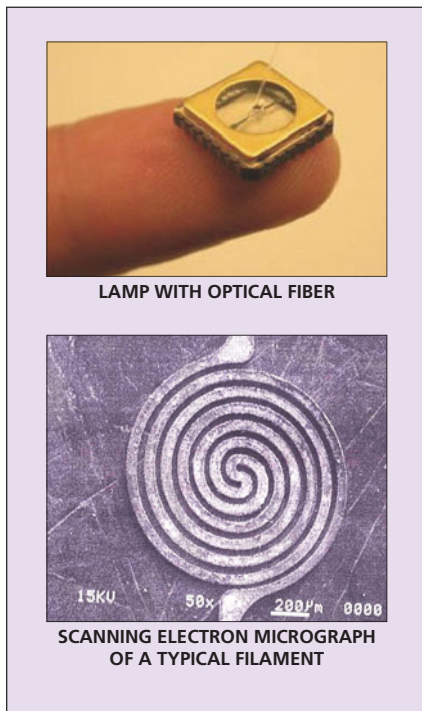
These lamps can be used without coupling optics.

John H. Glenn Research Center, Cleveland, Ohio

Miniature incandescent lamps of a special type have been invented to satisfy a need for compact, rapid-response, rugged, broadband, power-efficient, fiber-optic-coupled light sources for diverse purposes that could include cali-

brating spectrometers, interrogating optical sensors, spot illumination, and spot heating. A lamp of this type (see figure) includes a re-entrant planar spiral filament mounted within a ceramic package heretofore normally used to

house an integrated-circuit chip. The package is closed with a window heretofore normally used in ultraviolet illumination to erase volatile electronic memories. The size and shape of the filament and the proximity of the fila-



An **Extremely Compact Lamp** containing a spiral filament can be coupled directly to an optical fiber.

ment to the window are such that light emitted by the filament can be coupled efficiently to an optical fiber without intervening optics.

The components used for fabricating a lamp of this type are, more specifically, the following:

- The ceramic package is an appropriately sized commercially available leadless chip carrier containing gold contact pads. The package is chosen to

have a contact-pad spacing of about 0.25 in. (≈ 6 mm) so that the filament fits between two of the pads.

- The window is part of a windowed lid for the leadless chip carrier, supplied with a preform made of gold/tin solder. The preform is to be used subsequently in bonding (by soldering) the lid to the leadless chip carrier.
- The filament is formed by chemical etching or laser ablation of a 25- μm -thick sheet of tungsten or a tungsten/rhenium alloy.
- Two commercially available contact-pad brazing preforms made of a silver/copper/indium/titanium alloy that has a liquidus temperature of 715 °C are needed for attaching (by brazing) the filament to two contact pads.

Once the aforementioned components have been prepared, the lamp is assembled as follows:

1. The brazing preforms are placed on two opposing contact pads.
2. The outer ends of the filament are placed on the brazing preforms.
3. The assembly as described thus far is placed in either a vacuum furnace at a pressure of 10^{-7} torr (1.3×10^{-5} Pa) or a furnace containing an inert atmosphere, and heated to ≈ 800 °C or until brazing alloy melts and wets the filament.
4. The assembly is cooled to harden the braze, then the furnace is opened to room air and the assembly is removed from the furnace.
5. Optionally, at this point, the assembly can be placed in a vacuum chamber, wherein the filament can be baked

out by applying operating power to it. The assembly is then removed from the vacuum chamber.

6. A small nick is made in the solder preform on the lid to allow air to escape during step 8.
7. The lid is placed on the ceramic package, held in place by a weight or a clip. The package is placed in a vacuum furnace.
8. The vacuum furnace is pumped down to the desired vacuum for the interior of the lamp.
9. The furnace is heated to the eutectic temperature of the solder to melt and reflow the solder, then is cooled back to room temperature, then opened to air.

Lamps of this type containing tungsten and tungsten/rhenium filaments have been operated in laboratory tests at temperatures up to 2,650 and 2,725 °C, respectively. At an input power of ≈ 2 W, each lamp generates a luminous flux of about 1.5 lumens.

This work was done by Margaret Tuma of Glenn Research Center; Joe Collura of the Lighting Innovations Institute; Henry Helvajian of the Aerospace Corp.; and Michael Pocha, Glenn Meyer, Charles F. McConaghy, and Barry L. Olsen of Lawrence Livermore National Laboratory. Further information is contained in a TSP (see page 1).

Inquiries concerning rights for the commercial use of this invention should be addressed to NASA Glenn Research Center, Innovative Partnerships Office, Attn: Steve Fedor, Mail Stop 4-8, 21000 Brookpark Road, Cleveland, Ohio 44135. Refer to LEW-17820-1.

Bidirectional Pressure-Regulator System

This system can be used in regenerative fuel cell systems.

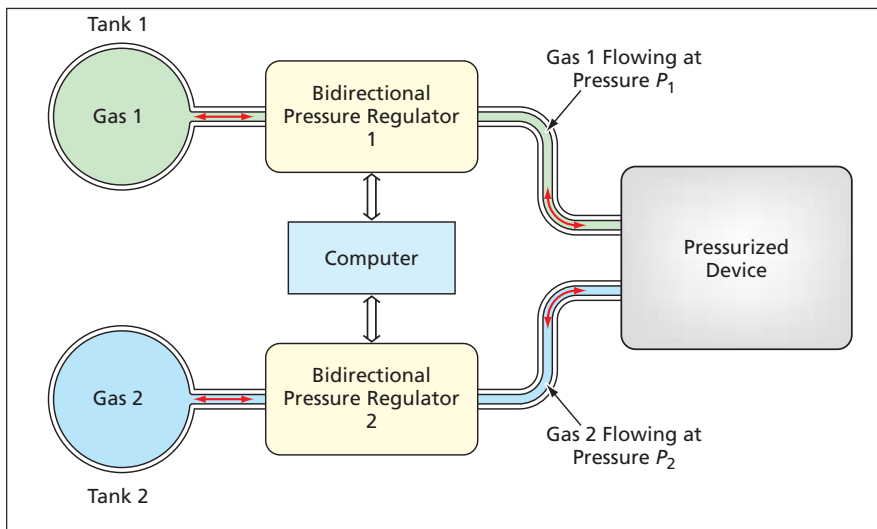
John H. Glenn Research Center, Cleveland, Ohio

A bidirectional pressure-regulator system has been devised for use in a regenerative fuel cell system. The bidirectional pressure-regulator acts as a back-pressure regulator as gas flows through the bidirectional pressure-regulator in one direction. Later, the flow of gas goes through the regulator in the opposite direction and the bidirectional pressure-regulator operates as a pressure-reducing pressure regulator. In the regenerative fuel cell system, there are two such bidirectional regulators, one for the hydrogen gas and another for the oxygen gas. The flow of gases goes from the regenerative fuel cell system

to the gas storage tanks when energy is being stored, and reverses direction, flowing from the storage tanks to the regenerative fuel cell system when the stored energy is being withdrawn from the regenerative fuel cell system. Having a single bidirectional regulator replaces two unidirectional regulators, plumbing, and multiple valves needed to reverse the flow direction. The term "bidirectional" refers to both the bidirectional nature of the gas flows and capability of each pressure regulator to control the pressure on either its upstream or downstream side, regardless of the direction of flow.

The system includes a computer that runs software formulated specifically to control the operation of the bidirectional pressure regulators. Each bidirectional pressure regulator includes the following components:

- A ten-turn needle valve;
- Two pressure sensors on opposite sides (upstream and downstream) of the valve;
- A stepping motor, connected to the shaft of the needle valve, for increasing or decreasing the valve orifice size as needed to decrease or increase the difference between the upstream and downstream pressures;



The Bidirectional Pressure-Regulator System regulates pressures P_1 , P_2 , and $P_2 - P_1$.

- A ten-turn potentiometer for providing valve-position feedback to the software; and
- Interface circuits between the computer and the stepping motor, pressure transducers, and potentiometer.

The software provides a capability for modifying set points for either upstream or downstream pressure during operation to adjust to changing flow condi-

tions, and/or to other changing system conditions, including changing pressure-control requirements. In addition, the software can easily be modified for application to different closed gas-flow systems. The performance of the bidirectional pressure regulator can be modified by the selection of the valve, the pressure transducers, the stepping motor, and the control parameters em-

bedded within the software control code.

In traditional pressure-regulation practice, control of a differential pressure between two gases would typically involve the use of plumbing to couple the pressures of the gases to a differential-pressure-sensing device; such a device is said to be “hardplumbed.” In contrast, the bidirectional-pressure-regulator system can be said to be “soft-plumbed” because the connection between the pressures of the two gases is made only in software. In the event that the two gases are such as to pose a risk of fire, explosion, or toxicity if allowed to mix, soft plumbing offers an important safety advantage over hard plumbing by eliminating a potential source of leakage and mixing.

This work was done by Kenneth Burke and John R. Miller of Glenn Research Center and Ian Jakupca and Scott E. Sargi of Analex Corp. Further information is contained in a TSP (see page 1).

Inquiries concerning rights for the commercial use of this invention should be addressed to NASA Glenn Research Center, Innovative Partnerships Office, Attn: Steve Fedor, Mail Stop 4-8, 21000 Brookpark Road, Cleveland, Ohio 44135. Refer to LEW-17548-1.

Prism Window for Optical Alignment

Prism windows could be generally useful in manufacture of optical instruments.

NASA's Jet Propulsion Laboratory, Pasadena, California

A prism window has been devised for use, with an autocollimator, in aligning optical components that are (1) required to be oriented parallel to each other and/or at a specified angle of incidence with respect to a common optical path and (2) mounted at different positions along the common optical path. The prism window can also be used to align a single optical component at a specified angle of incidence. Prism windows could be generally useful for orienting optical components in manufacture of optical instruments.

Heretofore, for aligning multiple optical components in a large optical assembly for which there is a requirement that no such component completely obstruct the alignment optical path to any other such component, it has been common practice to use a single large-aperture autocollimator or interferometer. However, the sizes of optical assemblies amenable to this alignment practice are limited by

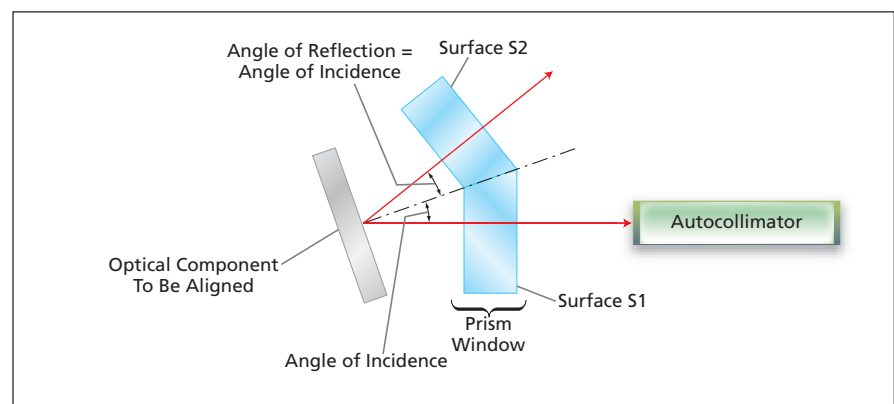


Figure 1. A Prism Window comprising two beam-splitter windows bonded together at a predetermined angle equal to twice a specified angle of incidence is used in conjunction with an autocollimator to align an optical component at the specified angle of incidence.

the sizes of apertures of commercially available autocollimators and interferometers. Moreover, in some cases, it may be necessary to remove some optical components to prevent obscuration of other optical components or to make room for

the autocollimator or interferometer. In contrast, the prism window makes it possible to use an autocollimator or other suitable instrument of narrow aperture to align multiple optical components in a possibly large optical assembly, without

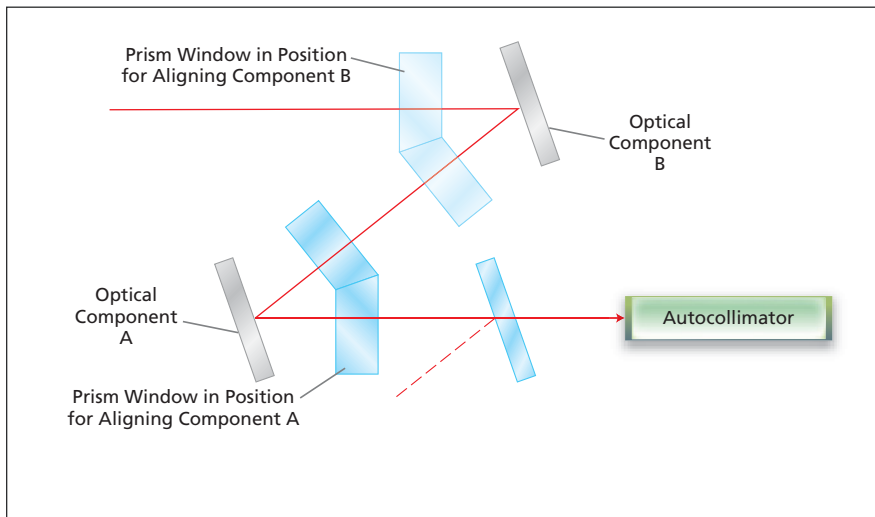


Figure 2. **Multiple Optical Components** are aligned in the manner of Figure 1 by repetition of the basic alignment procedure with the prism window suitably positioned in relation to each component to be aligned.

need to remove one or more optical components to prevent obscuration of other optical components or to make room for the alignment instrumentation.

“Prism window” as used here should not be confused with “prism window” used in U.S. Patent 4,772,094 to denote an assembly of prisms configured as a stereoscopic viewing device. Instead, as used here, “prism window” denotes an application-specific unit comprising two beam-splitter windows that are

bonded together at an angle chosen to obtain the specified angle of incidence.

Figure 1 illustrates a simple example of the use of a prism window and an autocollimator to align one optical component in a horizontal plane of incidence. In this example, the autocollimator is nominally aimed horizontally and the prism window is mounted on a flat, smooth, nominally horizontal platform that can be adjusted slightly in rotation about any or all of three axes to bring

the prism window into alignment with the autocollimator.

First, the surface S1 of the prism window is aligned with the autocollimator by performing such adjustments while using the autocollimator in the conventional manner to center light reflected from surface S1. Next, surface S2 is brought into alignment by rotating the platform about the axis parallel to the optical axis of the collimator until the table is as nearly level as possible, as indicated by a commercial level meter or any other suitable means. Finally, the optical component to be aligned is placed at or near the desired position and adjusted in tilt and tip. Alignment of this component is deemed to be achieved when, as observed via the autocollimator, light reflected from surfaces S1 and S2 is centered.

Figure 2 illustrates an example of the use of a prism window in conjunction with an autocollimator to align multiple optical components with respect to a multi-leg common optical path. In this case, the procedure described above for the single-component case must be repeated, with appropriate positioning of the prism window with respect to each component to be aligned.

This work was done by Hong Tang of Caltech for NASA’s Jet Propulsion Laboratory. Further information is contained in a TSP (see page 1). NPO-45546

Single-Grid-Pair Fourier Telescope for Imaging in Hard-X Rays and γ Rays

Images would be equal to or superior to those produced by multiple-grid-pair telescopes.

Marshall Space Flight Center, Alabama

The figure is a simplified depiction of a proposed Fourier telescope for imaging in hard-x rays and γ rays. This instrument would contain only one pair of grids made of an appropriate radiation-absorbing/scattering material, in contradistinction to multiple pairs of such as grids in prior Fourier x- and γ -ray telescopes. This instrument would also include a relatively coarse gridlike image detector appropriate to the radiant flux to be imaged. Notwithstanding the smaller number of grids and the relative coarseness of the imaging detector, the images produced by the proposed instrument would be of higher quality.

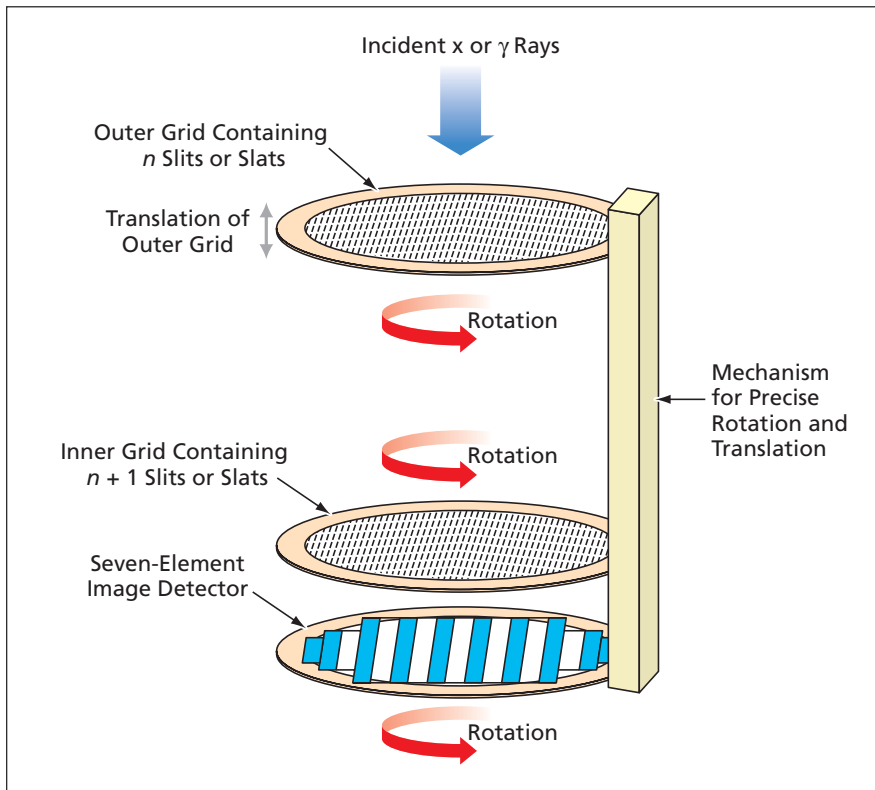
A mechanism that would include a gear drive would maintain a precise alignment between the grids and the

detector while stepping them through rotation and axial translation. The rotation would provide continuous two-dimensional coverage of the spatial frequencies of interest, while the slit widths of the grids and their axial translation would determine the range of magnitudes of the detected spatial frequencies. If the outer grid were translated, then there would be no need to translate the inner grid and the detector. To simplify the mechanism and the problem of maintaining alignment, the detector, its readout circuitry, and the associated image-data processor could be attached to the back of the inner grid.

Both grids would have the same overall width. If n were the number of slits

or slats in one of the grids, then the other grid must contain $n + 1$ slits, respectively. Because both grids would have the same overall width, the width of an individual slit or slat would be slightly greater in the n grid than in the $n + 1$ grid. It would not matter which grid was characterized by the greater number; for the initial design, n and $n + 1$ would be chosen for the outer and inner grid, respectively. The image detector could be composed of as few as two elements; however, prior research has shown that seven elements would represent a better compromise between the quality of image data and the complexity of the hardware.

Although practically any alignment could be used as long as it were known a



This Fourier X-Ray/ γ -Ray Telescope would contain only one pair of parallel absorbing/scattering grids, whereas prior such telescopes contain greater numbers of such grids.

priori, it would be convenient to align the middle element of the detector with the central slits of the inner and outer grids. With this alignment, a point source on the axis of symmetry of the telescope would produce a fringe pattern having peak intensity on the middle detector element. As the point source moved off the axis, the fringe pattern would shift accordingly, enabling acquisition of data on the amplitude and phase of the spatial-frequency component corresponding to the slit width, distance between grids, and grid angle. The processor would sum the photon counts on the detector elements to produce a four-parameter output data stream indicative of the intensity and location of the peak amplitude on the detector (equivalently, of magnitude and phase) as functions of the angle of rotation and the distance between the grids.

This work was done by Jonathan Campbell of Marshall Space Flight Center.

This invention is owned by NASA, and a patent application has been filed. For further information, contact Sammy Nabors, MSFC Commercialization Assistance Lead, at sammy.a.nabors@nasa.gov. Refer to MFS-31805-1.

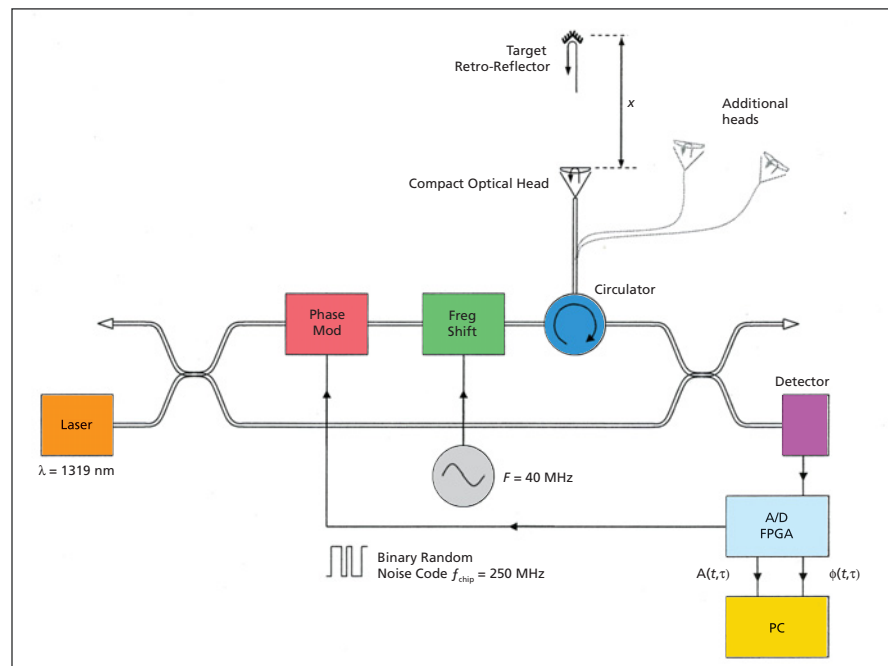
Range-Gated Metrology With Compact Optical Head

A compact, single-fiber optical head requires minimal internal alignment.

NASA's Jet Propulsion Laboratory, Pasadena, California

This work represents a radical simplification in the design of the optical head needed for high-precision laser ranging applications. The optical head is now a single fiber-optic collimator with dimensions of order of 1×2 cm, which can be easily integrated into the system being measured with minimal footprint. Previous heads were significantly larger, with multiple optical elements requiring careful alignment. The new design has only one optical fiber per head, rather than four, making it much easier to multiplex between tens or hundreds of heads. It is capable of subnanometer precision, consistent with the demanding requirements of new missions.

By combining a large number of multiplexed, low-cost, ultra-compact optical heads, it will be possible to form dense optical trusses, with minimal footprint, for the stabilization of large precision structures. The compact heads could be integrated with a piezoelectric actuator inside a tube to provide an "active strut"



A schematic of the Range-Gated Metrology System.

— a lightweight, structural member with infinite stiffness and zero thermal expansion — which can form the basis for extremely stable, lightweight structures. The compact heads could also be used as a tool in the laboratory for monitoring vibration and drifts in the dimensions of an experiment. Laser metrology may thus attain the same level of utility as accelerometers and thermistors. Simple magnetic or snap-on mounts could be used to position and point the heads and target retro-reflectors.

This advance in optical-head design is enabled by the application of pseudo-random noise (PRN) codes to optical metrology systems. This code is used to

discriminate between multiple optical returns that have different propagation delays. In this way, the phase of the signal from the reference surface on the optical head can be measured independently of the phase of the signal from the more distant target retro-reflector.

A prototype system has been assembled in the laboratory. The data were recorded on a digital oscilloscope, and the signal processing was applied off-line in software. Future work will include the implementation of the software algorithms in a real-time FPGA-based signal processing system, and the demonstration of different multiplexing schemes.

This work was done by Serge Dubovitsky,

Daniel Shaddock, Brent Ware, and Oliver Lay of Caltech for NASA's Jet Propulsion Laboratory. Further information is contained in a TSP (see page 1).

In accordance with Public Law 96-517, the contractor has elected to retain title to this invention. Inquiries concerning rights for its commercial use should be addressed to:

*Innovative Technology Assets Management
JPL*

Mail Stop 202-233

4800 Oak Grove Drive

Pasadena, CA 91109-8099

E-mail: iaoffice@jpl.nasa.gov

Refer to NPO-45102, volume and number of this NASA Tech Briefs issue, and the page number.



Lossless, Multi-Spectral Data Compressor for Improved Compression for Pushbroom-Type Instruments

A modified data compression algorithm could be used on commercial satellites or other applications with multispectral imaging instruments.

NASA's Jet Propulsion Laboratory, Pasadena, California

A low-complexity lossless algorithm for compression of multispectral data has been developed that takes into account pushbroom-type multispectral imagers' properties in order to make the file compression more effective. These types of imagers use a detector array to acquire data in spatial-spectral slices. Each detector element corresponds to a specific spectral band and cross-track position. Because the characteristics of detector elements generally vary somewhat from element to element, cross-track adjacent samples in a given spectral band are not as similar as they are in an instrument that uses the same detector for all samples in a given spectral band (e.g. in a whiskbroom-type instrument). Along-track adjacent samples will tend to be very similar.

Therefore, the fast lossless algorithm described in "Fast Lossless Compression of Multispectral-Image Data" (NPO-42517), *NASA Tech Briefs*, Vol. 30, No. 8 (August 2006), pages 26-28 was modified in two ways to increase the compression efficiency for these imagers. The first modification involves a local mean that was originally computed, for each sample, as the average sample value in a causal neighborhood of four adjacent samples

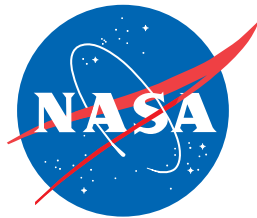
within the spectral band. Local means are subtracted from sample values to produce the input quantities for the adaptive filtering algorithm. For data from pushbroom-type multispectral imagers, it is found that letting the local mean be equal to the previous sample in the same cross-track position (and in the same spectral band) gave significantly better results. Specifically, for all rows (along-track positions) except the first row in a segment, the local mean equals the previous sample in the same cross-track position. For the first row in a segment, no such sample is available, so the local mean equals the causal cross-track adjacent sample. In addition, the prediction neighborhood of the sample is changed. In the original algorithm, this neighborhood contains three samples from the same band as the given sample, and one sample from each of the three preceding spectral bands. Under this first modification, only the first three samples from the three preceding spectral bands are used.

For the second modification, crude calibration information is used as side information for the compressor. This modification exploits the observation that the variations in detector element

characteristics are an inherent property of the detector, and there is little change in this variation over time. A key ingredient in this modification is a calibration array containing approximate, constant offsets for the detector elements. Each sample in a data set has the corresponding calibration value subtracted prior to starting compression, and the decompressor reverses this process after decompression. It is noted that the decompressor requires a copy of the calibration information. There are various ways in which the calibration array might be generated. In this instance, only a single calibration array was generated, but it appeared to work well with a large number of datasets from the same instrument.

When used with the first modification, the second modification primarily only affects how the first line of each segment is compressed. Nevertheless, the improvement for this line is significant enough to provide a noticeable, overall compression improvement.

This work was done by Matthew Klimesh of Caltech for NASA's Jet Propulsion Laboratory. Further information is contained in a TSP (see page 1). NPO-45473



National Aeronautics and
Space Administration